

This is an Open Access document downloaded from ORCA, Cardiff University's institutional repository: <https://orca.cardiff.ac.uk/id/eprint/135680/>

This is the author's version of a work that was submitted to / accepted for publication.

Citation for final published version:

Chaminda Bandara, W. G., Godaliyadda, G. M. R. I., Ekanayake, M. P. B. and Ekanayake, J. B. 2020. Coordinated PV re-phasing: a novel method to maximize renewable energy integration in LV networks by mitigating network unbalances. *Applied Energy* 280 , 116022. 10.1016/j.apenergy.2020.116022

Publishers page: <http://dx.doi.org/10.1016/j.apenergy.2020.116022>

Please note:

Changes made as a result of publishing processes such as copy-editing, formatting and page numbers may not be reflected in this version. For the definitive version of this publication, please refer to the published source. You are advised to consult the publisher's version if you wish to cite this paper.

This version is being made available in accordance with publisher policies. See <http://orca.cf.ac.uk/policies.html> for usage policies. Copyright and moral rights for publications made available in ORCA are retained by the copyright holders.



Coordinated PV re-phasing: a novel method to maximize renewable energy integration in LV networks by mitigating network unbalances

W.G. Chaminda Bandara^a, G.M.R.I. Godaliyadda^a, M.P.B. Ekanayake^a, J.B. Ekanayake^{*,ab}

^aDepartment of Electrical and Electronic Engineering, University of Peradeniya, Peradeniya (20400), Sri Lanka.

^bSchool of Engineering, Cardiff University, The Parade, Cardiff CF24 3AA, United Kingdom.

Highlights

- Maximize renewable energy penetration through coordinated re-phasing of solar PV.
- An automatic PV re-phasing switch that can connect to single-phase PV inverters.
- A modified DBFOA to determine the optimum phase combination of PV systems.
- The key mechanisms of DBFOA are modified to cater to PV re-phasing problem.
- A contextually optimized initializer to improve the convergence speed of DBFOA.

Abstract

As combating climate change has become a top priority and as many countries are taking steps to make their power generation sustainable, there is a marked increase in the use of renewable energy sources (RESs) for electricity generation. Among these RESs, solar photovoltaics (PV) is one of the most popular sources of energy connected to LV distribution networks. With the greater integration of solar PV into LV distribution networks, utility providers impose caps to solar penetration in order to operate their network safely and within acceptable norms. One parameter that restricts solar PV penetration is unbalances created by loads and single-phase rooftop schemes connected to LV distribution grids. In this paper, a novel method is proposed to mitigate voltage unbalance in LV distribution grids by optimally re-phasing grid-connected rooftop PV systems. A modified version of the discrete bacterial foraging optimization algorithm (DBFOA) is introduced as the optimization technique to minimize the overall voltage unbalance of the network as the objective function, subjected to various network and operating parameters. The impact of utilizing the proposed PV re-phasing technique as opposed to a fixed phase configuration are compared based on overall voltage unbalance, which was observed hourly throughout the day. The case studies show that the proposed approach can significantly mitigate the overall voltage unbalance during the daytime and can facilitate to increase the usable PV capacity of the considered network by 77%.

Keywords: Renewable energy integration, Rooftop solar PV, PV re-phasing, network unbalance, LV distribution networks, Bacterial foraging optimization.

* Corresponding author.

Email addresses: chaminda.bandara@eng.pdn.ac.lk (W.G. Chaminda Bandara), roshangodd@ee.pdn.ac.lk (G.M.R.I. Godaliyadda), mpb.ekanayake@ee.pdn.ac.lk (M.P.B. Ekanayake), jbe@ee.pdn.ac.lk, ekanayakej@cardiff.ac.uk (J.B. Ekanayake*)

List of Abbreviations

ACO	Ant Colony Optimization
ADN	Active Distribution Network
APF	Active Power Filter
BFOA	Bacterial Foraging Optimization Algorithm
BF-SD	Bacterial Foraging-Spiral Dynamic
CPN	Colored Petri nets
CPU	Central Processing Unit
DBFOA	Discrete Bacterial Foraging Optimization
DG	Distributed Generators
DFR	Distribution Feeder Reconfiguration
DGA	Discrete Genetic Algorithm
DSS	Distribution System Simulator
DVR	Dynamic Voltage Restorer
FPV	Floating PV
GA	Genetic Algorithm
GPV	Ground-mounted PV
HS	Heuristic Search
IEC	International Electrotechnical Commission
LV	Low Voltage
LVDG	Low Voltage Distribution Grid
MV	Medium Voltage
PV	Photovoltaic
PWM	Pulse Width Modulation
RES	Renewable Energy Sources
RMS	Root Mean Square
SA	Simulated Annealing
SCADA	Supervisory Control and Data Acquisition
SFLA	Shuffled Frog Leaping Algorithm
SOP	Soft Open Points
SOCP	Second-Order Cone Programming
S-MILP	Stochastic Mixed-Integer Linear Programming
VUF	Voltage Unbalance Factor

Nomenclature

\mathbb{H}_{VU}^i	Highest unbalance region in the network
i	Index of i -th PV configuration vector
j	Incremental counter (index) for D-Chemotaxis step
J_C^i	Cumulative cost of i -th PV configuration vector
J_{last}	Best cost recorded
$J(i, j, k, l)$	Cost of i -th PV configuration vector at j -th D-Chemotaxis step, k -th D-Reproduction step and l -th D-Elimination Dispersal step
$J(\mathbf{x})$	Penalized objective function
k	Incremental counter (index) for D-Reproduction step
k_n	Radius of the highest unbalance region
k_R	Number of phase combinations having smallest active power mismatch
l	Incremental counter (index) for D-Elimination Dispersal step
$n_{VUF_{max}}$	Busbar with the highest voltage unbalance
N	Total number of busbars in the network
N_C	Number of D-Chemotaxis steps
N_{pv}	Number of grid-connected PV systems in the network
N_r	Maximum number of random phase changing steps performed
N_{re}	Number of D-Reproduction steps
P_{ed}	D-Elimination Dispersal probability
r	Incremental counter (index) for the random phase changing step
RN^i	A random number between 0 and 1
S	Number of PV configuration initializers
\overline{VUF}	Mean voltage unbalance factor
VUF_{max}	Specified maximum unbalance level
VUF_n	Voltage unbalance factor at n -th busbar

V_{max}	Specified maximum phase voltage magnitude
V_{min}	Specified minimum phase voltage magnitude
V_n^-	Negative sequence voltage component at n-th busbar
V_n^+	Positive sequence voltage component at n-th busbar
V_n^a	Voltage magnitude of phase-a at n-th busbar
V_n^b	Voltage magnitude of phase-b at n-th busbar
V_n^c	Voltage magnitude of phase-c at n-th busbar
\mathbf{x}	PV configuration vector
x_m	m-th element of the PV configuration vector
$\mathbf{x}^i(j, k, l)$	i-th PV configuration vector at j-th D-Chemotaxis step, k-th D-Reproduction step and l-th D-Elimination Dispersal step
Z^{abcn}	Impedance matrix for the overhead cable
$\mu_{V_n^a}$	Penalty function for voltage magnitude of phase-a
$\mu_{V_n^b}$	Penalty function for voltage magnitude of phase-b
$\mu_{V_n^c}$	Penalty function for voltage magnitude of phase-c
μ_{VUF_n}	Penalty function for voltage unbalance

1. Introduction

With the de-carbonization agenda of many countries, the integration of renewable energy sources (RES) such as solar and wind energy into the power system has increased considerably. Among these RES, photovoltaic solar energy (PV) is one of the fastest-growing renewable energy sources with an annual growth rate of 35 to 40% [1]. At the end of 2019, the global cumulative solar energy capacity stood at 580 GW. These installations come in three forms: ground-mounted PV (GPV) [2, 3], floating PV (FPV) [4, 5], and rooftop PV [6,7]. As GPV and FPV use dedicated feeders for connection to the network, there is no local impact on the network, whereas the random installation of small-size rooftop PV systems in LV networks causes a voltage unbalance. The unbalance in the phase voltages and the resulting flow of large neutral currents can increase the distribution and transformer losses due to overheating and can overload the neutral conductor [8,9]. Due to these consequences of voltage unbalance, utility providers limit the usable PV capacity that they can accommodate for LV networks [10–12]. Therefore, an effective solution is needed to improve the future integration of solar PV sources into LV networks. How to effectively reduce the unbalance is a long-standing question, and much effort has been devoted to answering this question in the past decade.

Table 1 summarizes the various approaches proposed in the literature in order to minimize network unbalance along with their advantages and limitations. As can be seen from Table 1, these techniques can be mainly divided into two categories [13]. The first category mitigates the network unbalance by using neutral current compensation devices such as passive harmonic filters and specially designed active power filters. The second category is based on distribution network reconfiguration techniques and can be divided into two: distribution feeder reconfiguration (DFR) and phase balancing. It is important to note that both DFR and phase balancing techniques use non-linear, non-differentiable, highly combinatorial, and constrained optimization algorithms to find the optimal solution [14].

The neutral current compensation devices do not mitigate the network imbalance, but they filter excess neutral current flowing through the neutral conductor. In [15], a synchronous machine has been used to filter out all the zero-sequence harmonic currents of the neutral. Apart from the synchronous machines, different transformer topologies have also been analyzed by the researches to compensate neutral current. Commonly used topologies to reduce the neutral current are a zig-zag transformer [16], a star-delta transformer [17], T-connected transformer [18] and, star-hexagon transformer constructed from three single-phase three-winding transformers [19]. Nowadays, power-electronic-based compensators such as H-bridge shunt Active Power Filter (APF) [20], capacitor midpoint APF [21], and three-phase four-wire four-leg APF [22], and Dynamic Voltage Restorer (DVR) [23] have also been used to overcome neutral current and other power quality problems. However, all of the aforementioned methods reduce only the neutral current but cannot reduce total power loss, voltage, or current unbalance. Hence, many researchers have used DFR techniques to mitigate system-level unbalance and power losses.

The DFR technique optimizes the open or closed status of sectionalizing switches and tie switches to transfer the loads from overloaded feeders to the lightly loaded feeders in order to minimize

desired objective functions (e.g., voltage unbalance, load unbalance, power loss, etc.) [24]. Many researchers have used different optimization techniques to identify the optimum states of the sectionalizing and/or tie switches. In [25], a heuristic search methodology has been utilized for the feeder reconfiguration problem. In [26], Ant Colony Optimization (ACO) along with Graph Theory has been used to determine the optimum status while maintaining the system radiality. In [27], a method to convert distribution network reconfiguration problem into a spanning tree of the graph is proposed, then an improved ACO algorithm is utilized to solve the reconfiguration problem. In [28], the genetic algorithm (GA) is utilized for the reconfiguration problem using a composite multi-objective function of power loss saving, voltage profile, voltage unbalance and current unbalance of the system. In [29], a multi-objective evolution programming method with adapted weight calculation is applied in order to overcome the weakness of the traditional GAs [30,31]. In [32], a combined optimization technique has been developed with heuristic rules and fuzzy logic for efficiency and robust performance. A hybrid optimization algorithm based on fuzzy logic and Bees algorithm is also used in reconfiguration and multiple DG placement [33]. In addition, a Colored Petri nets (CPN) inference mechanism-based distribution feeder load balancing technique has been proposed in [34]. An improved version of an aforementioned CPN optimization algorithm is proposed in [35]. Recently, an enhanced second-order cone programming (SOCP)-based method for load balancing using multi-terminal soft open points (SOP) has been proposed in [36]. An improved version of the aforementioned algorithm has been proposed in [37] which allocates SOPs and DG units simultaneously with and without network reconfiguration. In [38], a dynamic distribution network reconfiguration approach is proposed in the context of the active distribution network (ADN) under high penetration of distributed generations. In [39], an optimal network reconfiguration technique is formulated as a multi-objective stochastic mixed-integer linear programming (S-MILP) model. In [40], a new technique based on Bacterial Foraging with Spiral Dynamic (BF-SD) is applied for simultaneous optimization of re-phasing, reconfiguration, and DG placement. Although the aforementioned DFR techniques can only mitigate unbalance at the system level it cannot mitigate phase unbalance at the feeder level [13]. Hence, phase balancing techniques have been proposed to mitigate feeder level unbalance.

The phase balancing technique can be implemented in two ways: (1) load re-sequencing and (2) load re-phasing. In the load re-sequencing technique, the phase sequence at each busbar is re-sequenced to their optimal combination. To avoid any reverse operation of inductive loads, the positive and negative phase sequences are only taken into account [41]. In the load re-phasing technique, the loads from the overloaded phases are transferred to the lightly loaded phases by analyzing the current or power difference between the phases. To identify the optimum phase sequence for the three-phase loads and optimum phase combination for the single-phase loads, different optimization techniques have been proposed. In [42], a mixed-integer programming formulation for phase balancing optimization has been proposed. In [43], Simulated Annealing (SA) has been introduced as an effective method to solve the phase balancing problem while paying attention to the non-linear effects such as voltage drops and energy losses. In [44], an application program is developed which contains a function of load flow and phase balancing of feeders with phase re-phasing. In [45], A fuzzy logic-based phase balancing approach along with an optimization oriented expert system has been proposed for LVDGs. An advanced version of the aforementioned algorithm has been proposed in [46] in which the algorithm is extended for

both radial and meshed distribution networks in the presence of unbalanced loads. In [47] and [48], the economic feasibility of the phase balancing approach to mitigate network unbalance has been analyzed under the presence of plug-in battery electric vehicles changing and distributed energy storage systems. However, all of these phase balancing techniques have been tested on small LV networks with a few loads and have not been implemented in large LV networks due to the high computational time they use to identify the optimum solution. Also, the aforementioned unbalance mitigation techniques raise many concerns when they implemented in practical networks such as:

- *high initial cost* due to the fact that load switches need to be installed between the phases, at each end of the client [13],
- *several other indirect costs* such as the cost of customer interruption, the cost of customer reliability, etc. [47], and
- *possible harm or damage* to the customer equipment at the time of re-phasing.

Considering the above limitations of load re-phasing, in this paper, a PV re-phasing technique is proposed that only relies on the rooftop solar systems to minimize the network unbalance. Therefore, the re-phasing switches need to be installed only at the connection point of each rooftop solar system and require much fewer re-phasing switches per network as compared to load/feeder re-phasing techniques. Due to this low capital requirement for the implementation of the proposed PV re-phasing technique, it is ideal for the large-scale deployment in LV networks to minimize the network unbalance. Also, the proposed PV re-phasing technique has no impact on supply reliability and requires minimum or no customer interruption. Therefore, the proposed PV re-phasing technique is a more economical and effective way to minimize the network unbalance, and thereby facilitate to improve the integration of clean and renewable solar energy into the LV networks. The main contributions of this paper are listed as follows:

- ***A novel strategy to minimize unbalance in LV networks based on automatic re-phasing of grid-connected rooftop PV systems.*** The grid-connected rooftop solar systems are periodically re-phased to their optimal phase combination at pre-selected time intervals to minimize the system unbalance. The proposed PV re-phasing technique can maintain the voltage unbalance well below the 1% threshold line while simultaneously maintaining the phase voltages within their acceptable limits. This will help utility providers to allow more rooftop solar systems into the network without bothering about network unbalance. The case studies demonstrate that the proposed PV re-phasing strategy can improve the usable PV capacity of the considered network by 77%.
- ***A PV rephasing switch is proposed to perform automatic rephasing of grid-connected single-phase PV systems.*** Since the re-phasing switch only re-phases rooftop PV systems, not the loads or the feeders, it will not have any impact on supply reliability. Additionally, no customer interruption is required at the time of PV re-phasing.
- ***A discrete bacterial foraging optimization algorithm (DBFOA) was introduced to determine the optimal phase combination of grid-connected single-phase PV systems.*** The proposed DBFOA improves upon the classical BFOA by modifying the principal mechanisms of the classical method to specifically catered to the PV re-phasing problem, thereby increasing both convergence speed and accuracy. The proposed bacterial foraging

optimization algorithm determines the optimal phase combination for rooftop PV systems such that it will minimize the violations of voltage unbalance and phase voltage magnitudes.

The rest of the paper is organized as follows. Section 2 describes the structure of the proposed re-phasing switch and the overall operating mechanism of the PV re-phasing technique. Section 3 formulates the PV re-phasing problem. Section 4 describes the principal mechanisms of the proposed bacterial foraging optimization algorithm and the implementation details (i.e. the flow chart and the pseudo-code), as well as the simulation results, are given in section 5. Finally, section 6 presents our conclusions and future work.

Table 1: Summary of available techniques to mitigate network unbalances from the literature

Category	Technique	Examples	Advantages	Limitations
Neutral current compensating devices	<i>Passive filters and transformers</i>	Synchronous machines as filters [15]	<ul style="list-style-type: none"> • Not require any additional controller • Synchronous machine can be operated as a synchronous condenser (to reactive power control) and/or motor or generator. 	<ul style="list-style-type: none"> • Compensation characteristic depends on the zeros sequence impedance of the synchronous machine • High initial and maintenance cost • Bulky
		T connected transformer [18]	<ul style="list-style-type: none"> • Neutral current can be compensated to a large extent 	<ul style="list-style-type: none"> • Compensation characteristics are depending on the impedance of the transformer, location, and source voltage
		Star-hexagon transformer [19]	<ul style="list-style-type: none"> • Can reduce the zero-sequence harmonic current to a large extent 	
		Star-Delta transformer [17]	<ul style="list-style-type: none"> • Neutral current can be reduced to a large extent 	
		Zig-zag transformer [16]	<ul style="list-style-type: none"> • Neutral current can be reduced to a large extent 	<ul style="list-style-type: none"> • Neutral voltage variations may lead to abnormal operation of the load side.
	<i>Active power filters</i>	H-bridge shunt APF [20]	<ul style="list-style-type: none"> • Control can be done either as a three-phase unit or three separate single-phase units 	<ul style="list-style-type: none"> • Increased number of switching devices
		Three-phase four-wire capacitor	<ul style="list-style-type: none"> • Ability to reduce power quality problems 	<ul style="list-style-type: none"> • Voltage unbalance between the capacitors

		midpoint APF [21]	<ul style="list-style-type: none"> • Compensate not only the neutral current but also the harmonics from loads 	
		Three-phase, four-wire, four-leg APF [22]	<ul style="list-style-type: none"> • Most suitable for compensation of high neutral currents • Better controllability • Lower DC voltage requirement 	<ul style="list-style-type: none"> • Difficulty in controlling the four-leg inverter
Distribution network reconfiguration techniques	<i>Distribution feeder reconfiguration</i>	[24], [25], [26], [27], [28], [29], [30], [31], [32], [33], [34], [35], [36], [37], [38], [39], [40]	<ul style="list-style-type: none"> • Minimize load imbalance • Loss reduction • Congestion management • Increased hosting capacity in normal conditions • Capability to isolate fault areas by maintaining continuity of power supply to non-faulted areas 	<ul style="list-style-type: none"> • Only mitigate the system level unbalance and cannot mitigate the phase level unbalance
	<i>Phase balancing (load re-sequencing and load re-phasing)</i>	[41], [42], [43], [44], [45], [46]	<ul style="list-style-type: none"> • Ability to minimize phase level unbalance 	<ul style="list-style-type: none"> • A large number of re-phasing switches need to be installed • Require complex optimization techniques to find optimal phase combination for load switches

2. PV re-phasing arrangement

In this section, the structure of the re-phasing switch and the operating mechanism of automatic PV re-phasing in LV distribution grids are explained.

2.1. Structure of the PV re-phasing switch

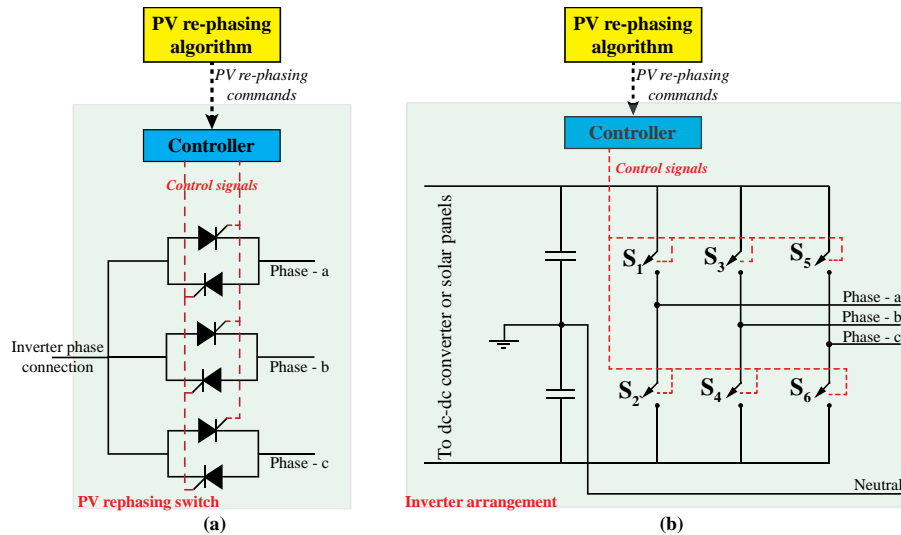


Figure 1: (a)-Thyristor switch, (b)-Inverter arrangement

Figure 1-(a) shows a schematic of a PV rephasing switch that can be connected to the output of the single-phase inverter. As can be seen, switching between phases can be achieved by blocking the already conducting pair of thyristors (or triac) and turning the pair of thyristors that are connected to the phase to which output should be connected. In order to avoid any circulating current between phases, a dead band should be introduced between the blocking signal and the turning on signal. However, this will eventually cause the PV inverter to take the start-up mode, thus, introducing an interruption of a few minutes (less than 3 min). This configuration is widely used for ac switching applications and its operation can be found in standard textbooks [49]. The thyristors used for this configuration should be able to continuously carry the maximum current that the PV plant generates. The main drawbacks are the continuous on-state loss (equal to the square of the current times dynamic resistance of the thyristor) and the extra cost due to the introduction of three back-to-back thyristors and its control circuits.

The inverter in Figure 1-(b) shows an alternative rephasing arrangement that can be used for nanosecond level transients from one phase to another. In this arrangement, a half-bridge inverter is used to convert dc into ac. If the output needs to be connected to Phase - a then switches S_1 and S_2 are operated in a complementary manner using a PWM switching pattern and all the other switches are blocked. If the output needs to be connected to Phase - b then S_1 and S_2 will be blocked and S_3 and S_4 will be turned on. Even though the presence of two extra arms incurs an additional cost, there are no additional losses due to the introduction of two more arms. The same arrangement can be introduced for full-bridge single-phase inverters.

When the above arrangements are employed for PV rephasing, switching from one phase to another will take place throughout the day and power electronic switches will experience transient switching. A similar arrangement as Figure 1-(a) is used in power factor correction capacitors, which switches the capacitors depending on the power factor of the load, many times a day, and they have proven to be robust under such frequent switching operations for many decades. This additional switching transient that operates on switches in Figure 1-(b) will not have any impact on switches as they are anyway switched at 5-10 kHz frequency by PWM during normal operation.

2.2. The architecture of the automatic PV re-phasing arrangement

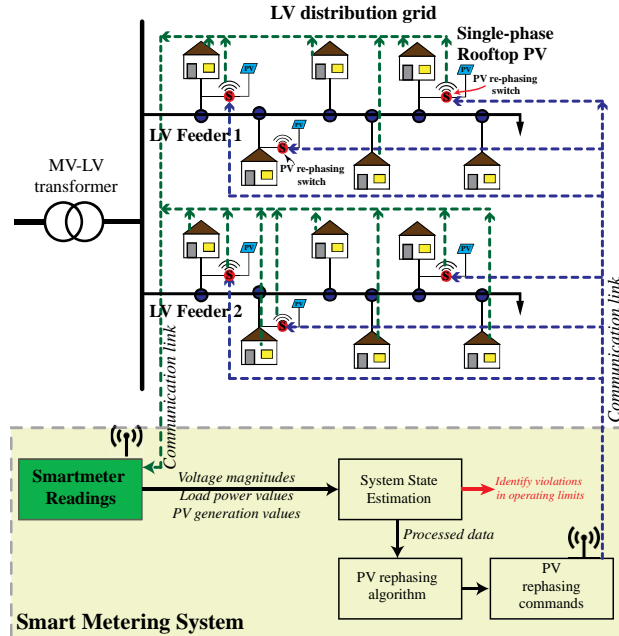


Figure 2: Schematic of the automatic PV re-phasing arrangement

Figure 2 shows the operating mechanism of the proposed PV re-phasing strategy. The necessary data such as PV generations and load demands are measured from smart meters and transmitted to the smart metering system. Typically, these smart meter measurements are subjected to different types of systematic, random, and communication errors [50,51]. Therefore, in the next step, state estimation is performed to detect the presence of bad data. These preprocessed smart meter data are sent to the PV re-phasing algorithm to determine the optimal phase combination of grid-connected PV systems, such that the overall voltage unbalance of the network is minimized. Finally, the re-phasing program transmits the required phase changes of PV systems through the smart metering system to the installed PV re-phasing switches and the re-phasing operation is carried out.

The time required for a PV re-phasing operation depends on the time it takes to transmit smart meter data from consumers and producers to the smart metering system (about 4.7 sec under 112 OFDM Symbol Data Frame [52]), the time required for system state estimation (about 0.10 sec [53]), the time required to execute the PV rephasing algorithm (about 33.7 sec – see Table 8), and the time it takes to transmit PV rephasing commands from smart metering system to PV rephasing

switches (about 4.7 sec under 112 OFDM Symbol Data Frame [52]). Therefore, the need for a PV re-phasing operation can be detected and then successfully executed in approximately 43.2 seconds. As mentioned in section 2.1, the actual operation of the PV rephasing switches could vary from 3 min for the topology shown in Figure 1-(a) to a few nanoseconds for the topology shown in Figure 1-(b).

3. Problem formulation

The aim of this work is to develop a strategy to minimize the overall voltage unbalance of the network such that the power quality and the reliability of the distribution system can be improved. The objective of this optimization problem can be expressed as the minimization of the mean voltage unbalance factor (\overline{VUF}) of the network as in,

$$\overline{VUF} = \frac{1}{N} \sum_{n=1}^N VUF_n \quad (1)$$

where, VUF_n is the voltage unbalance factor at n -th busbar and N is the total number of busbars in the network.

Subjected to the constraints:

1. Voltage unbalance at each busbar (VUF_n) must be strictly below the specified maximum unbalance level (VUF_{max}):

$$VUF_n \leq VUF_{max} \quad (2)$$

for $n = 1, 2, 3, \dots, N$.

2. Phase voltage magnitudes (V_n^a, V_n^b , and V_n^c) must strictly between the upper (V_{max}) and lower (V_{min}) limits:

$$V_{min} \leq V_n^a, V_n^b, V_n^c \leq V_{max} \quad (3)$$

for $n = 1, 2, 3, \dots, N$, where, V_n^a, V_n^b and V_n^c are the voltage magnitudes of a, b , and c phases at n -th busbar, respectively.

Equation (1) corresponds to the objective function to be minimized and represents the overall voltage unbalance (\overline{VUF}) of the distribution network. The inequality in (2) considers a constraint for voltage unbalance factor and ensures individual voltage unbalance factors (VUF_n for $n = 1, 2, \dots, N$) are below the specified maximum value, VUF_{max} . The inequality in (3) deals with the constraints for voltage magnitudes. It ensures the phase voltages (V_n^a, V_n^b , and V_n^c) fall within the acceptable voltage limits (lower limit V_{min} and upper limit V_{max}). In this study, V_{min} was considered as 0.94 pu and V_{max} was considered as 1.06 pu. In other words, (2) and (3) define the feasible regions for voltage unbalance (VUF_n) and phase voltage magnitudes (V_n^a, V_n^b, V_n^c), respectively.

In order to minimize (1) while simultaneously satisfying the constraints (2) and (3), penalty functions were introduced. The main idea of these penalty functions is that an optimal PV configuration (i.e. the optimal solution) requires that constraints be active so that this optimal solution lies in the feasible regions for voltage unbalance and phase voltage magnitudes. To ensure this, a penalty is applied to possible solutions when constraints are not satisfied. Therefore, the aforementioned optimization problem was reformulated as the minimization of the penalized objective function, $J(\mathbf{x})$, given by,

$$J(\mathbf{x}) = \overline{VUF} + k_1 \sum_{n=1}^{n=N} \mu_{VUF_n} + k_2 \left(\sum_{n=1}^{n=N} \mu_{V_n^a} + \sum_{n=1}^{n=N} \mu_{V_n^b} + \sum_{n=1}^{n=N} \mu_{V_n^c} \right) \quad (4)$$

where,

the penalty function for voltage unbalance (μ_{VUF_n}) is given by:

$$\mu_{VUF_n} = \begin{cases} VUF_n - VUF_{max} & ; \text{when } VUF_n > VUF_{max} \\ 0 & ; \text{when } VUF_n \leq VUF_{max} \end{cases} \text{ for } n = 1, \dots, N \quad (5)$$

the penalty function for voltage magnitudes of phase-a ($\mu_{V_n^a}$) is given by:

$$\mu_{V_n^a} = \begin{cases} |V_n^a - V_{min}| & ; \text{when } V_n^a < V_{min} \\ 0 & ; \text{when } V_{min} \leq V_n^a \leq V_{max} \\ V_n^a - V_{max} & ; \text{when } V_n^a > V_{max} \end{cases} \text{ for } n = 1, \dots, N \quad (6)$$

the penalty function for voltage magnitudes of phase-b ($\mu_{V_n^b}$) is given by:

$$\mu_{V_n^b} = \begin{cases} |V_n^b - V_{min}| & ; \text{when } V_n^b < V_{min} \\ 0 & ; \text{when } V_{min} \leq V_n^b \leq V_{max} \\ V_n^b - V_{max} & ; \text{when } V_n^b > V_{max} \end{cases} \text{ for } n = 1, \dots, N \quad (7)$$

the penalty function for voltage magnitudes of phase-c ($\mu_{V_n^c}$) is given by:

$$\mu_{V_n^c} = \begin{cases} |V_n^c - V_{min}| & ; \text{when } V_n^c < V_{min} \\ 0 & ; \text{when } V_{min} \leq V_n^c \leq V_{max} \\ V_n^c - V_{max} & ; \text{when } V_n^c > V_{max} \end{cases} \text{ for } n = 1, \dots, N \quad (8)$$

\mathbf{x} is the PV configuration vector, and k_1 and k_2 are the constant imposed on the penalty functions. The graphical illustrations of these penalty functions are shown in Figure 3.

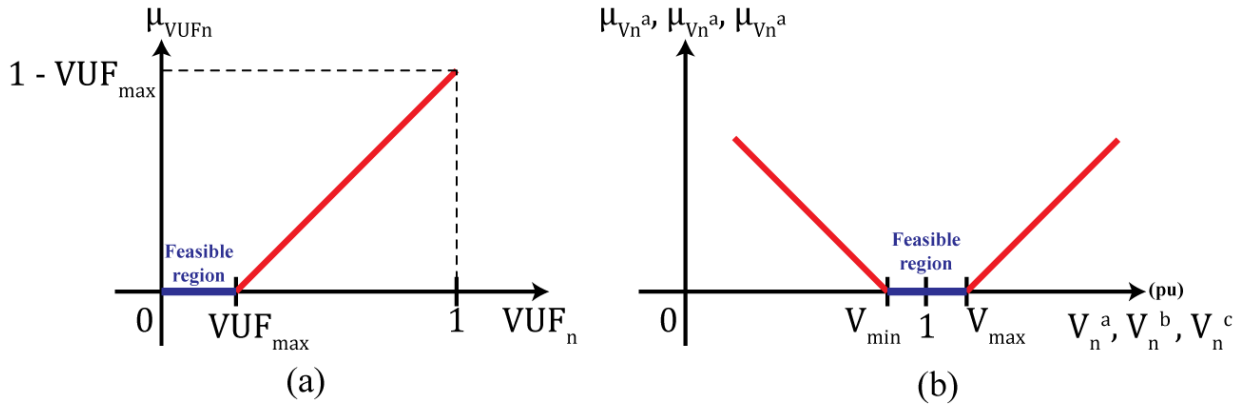


Figure 3: Penalty functions for (a) voltage unbalance and (b) phase voltage magnitudes.

The phase combination of grid-connected PV systems at a given time is represented by the *PV configuration vector*, \mathbf{x} . Therefore, for a network having N_{pv} number of grid-connected PV

systems, the PV configuration vector \mathbf{x} consists of N_{pv} number of phase entries where each phase entry corresponds to the phase of a grid-connected PV system in the network. Hence, each element (x_m) in the PV configuration vector- \mathbf{x} can take one of the three phases (*i.e.* $x_m \in \mathbb{P}$, $\mathbb{P} = \{a, b, c\}$). The format of the PV configuration vector is illustrated in Figure 4 with an example PV combination.

Format of the PV configuration vector $\mathbf{x} \in \mathbb{P}^{N_{pv}}$

Phase of PV_1	Phase of PV_2	Phase of PV_3	Phase of PV_m	Phase of $PV_{N_{pv}}$
-----------------	-----------------	-----------------	-----	-----	-----------------	-----	-----	-----	------------------------

Example PV configuration vector \mathbf{x}^i

Phase a	Phase b	Phase c	$x_m \in \mathbb{P}$	Phase a
---------	---------	---------	-----	-----	----------------------	-----	-----	-----	---------

Figure 4: The format of the PV configuration vector \mathbf{x}

It is important to note that there are different definitions available for the voltage unbalance factor; in this paper, the IEC definition [54] was used. In the IEC definition (IEC TR 61000-3-14:2011), the voltage unbalance factor is calculated as the ratio of negative sequence voltage component to the positive sequence voltage component and can be expressed as follows [54]:

$$VUF_n = \frac{V_n^-}{V_n^+} = \frac{\text{Negative sequence voltage component at } n^{\text{th}} \text{ busbar}}{\text{Positive sequence voltage component at } n^{\text{th}} \text{ busbar}} \times 100\% \quad (9)$$

The three-phase sequence voltage components were obtained by the symmetrical transformation. The steps for the computation of three-phase sequence voltage components from three-phase voltages can be found in [41].

4. Bacterial Foraging Optimization

Bacterial foraging optimization algorithm (BFOA) is a smart optimization technique that has proven to be very effective in search domains having several dimensions. BFOA is inspired by the social foraging behavior of *E. coli* bacteria. The underlying biology behind the foraging strategy of *E. coli* is emulated and used as a simple optimization algorithm [55,56]. In this paper, a discrete and adaptive version of BFOA is introduced to solve the PV re-phasing problem.

4.1. Concept of BFOA

During the foraging period, real bacteria achieve their motion with the help of their tensile flagella. Using these tensile flagella, bacteria can perform two basic motion types called tumble and swim. In the classical BFOA, the bacteria undergo *chemotaxis*, where they like to move towards nutrient gradient while avoiding the noxious environments. When they get enough food, they increase their length and under suitable temperature, they break in the middle to form an exact replica of itself. This phenomenon is called the event of *reproduction* in BFOA. However, due to the occurrence of sudden environmental changes or attacks, the chemotaxis progress may be destroyed, and a group of bacteria may move to some other place or some other mutation may be introduced to the bacteria population. This phenomenon is called the *elimination dispersal event* in BFOA, where all the bacteria in the region are killed or a group is dispersed into a new part of the environment.

References [55–61] provide a comprehensive analysis of the classical BFOA in different optimization problems.

4.2. Primary steps of the proposed DBFOA

The proposed DBFOA improves upon the classical BFOA by modifying the principal mechanisms to specifically handle the PV re-phasing problem. The modified versions of the principal mechanisms of the algorithm were named as *D-Chemotaxis*, *D-Reproduction*, and *D-Elimination dispersal*. The following subsections discuss these three principal mechanisms which drive the proposed DBFOA. The mapping of the terms in the PV re-phasing problem and the classical BFOA problem are shown in Table 2.

Table 2: Related terminology

Variable	Definition in PV rephrasing problem	Definition in classical BFOA
N_{pv}	The number of grid-connected PV systems in the network	The dimension of the search space
S	The number of PV configuration initializers	Total population of the bacterium
N_c	The number of D-chemotactic steps	The number of chemotactic steps
N_r	The maximum number of random phase changing steps performed	The swimming length
N_{re}	The number of D-Reproduction steps	The number of reproduction steps
P_{ed}	D-elimination dispersal probability	Elimination dispersal probability
i	i -th PV configuration vector	The i -th bacterium in the population
j	Incremental counter (index) for D-Chemotaxis step	Index for the chemotaxis step
k	Incremental counter (index) for D-Reproduction step	Index for the reproduction step
l	Incremental counter (index) for D-Elimination Dispersal step	Index of the elimination-dispersal event
r	Incremental counter (index) for the random phase changing step	Index for swimming step
$J(i, j, k, l)$	The cost of i -th PV configuration vector $\mathbf{x}^i(j, k, l)$	The cost at the location of the i -th bacterium $\mathbf{x}^i(j, k, l)$

4.2.1. Discrete Chemotaxis (D-Chemotaxis):

The D-Chemotaxis step updates the phase combination of a PV configuration vector such that the new phase combination has a lower cost value compared to its previous phase combination. In other words, the D-Chemotaxis step updates the phase combination in a direction corresponding to a gradient of decreasing cost value.

Here, the present phase combination in i -th PV configuration vector is given by $\mathbf{x}^i(j, k, l)$ and its updated version is denoted by $\mathbf{x}^i(j + 1, k, l)$ where, j , k , and l are the index for D-Chemotaxis, D-Reproduction, and D-Elimination dispersal, respectively.

The proposed D-Chemotaxis step first identifies the highest unbalance region (\mathbb{H}_{VU}^i) in the network corresponding to the phase combination in the i -th PV configuration vector, $\mathbf{x}^i(j, k, l)$. Here, the highest unbalance region is referred to the busbars within k_n number of busbars from the busbar with highest unbalance ($n_{VUF_{max}}$). Once the highest unbalance region \mathbb{H}_{VU}^i is identified, only the phase combinations of grid-connected PV systems in the highest unbalance region, \mathbb{H}_{VU}^i , are randomly changed to generate the updated phase combination, $\mathbf{x}^i(j + 1, k, l)$. This reduces the number of possible phase configurations greatly, while mitigating the impact of re-phasing on the overall network. However, the random change in the phases of PV systems in the highest unbalance region \mathbb{H}_{VU}^i does not guarantee that it finds a phase combination with a lower

cost value compared to its present phase combination $x^i(j, k, l)$ at once. Therefore, in such a situation, the random phase changing is repeated until it finds a suitable phase combination with lower-cost value, within a maximum of N_r iterations. If D-Chemotaxis is unable to find a phase combination with lesser cost value within the maximum N_r cycles, then the present phase combination $x^i(j, k, l)$ is retained as its updated phase combination $x^i(j + 1, k, l)$ as it is reasonable to assume that we have reached a low-cost point through random changes.

The pseudocode of the D-chemotaxis procedure is given in Algorithm 1 and the main steps are depicted in Figure 5.

Algorithm 1: D-Chemotaxis

- Step 1:** Perform a load flow analysis for the phase combination in i -th PV configuration vector, $x^i(j, k, l)$.
 - Step 2:** Evaluate the cost function- $J(i, j, k, l)$ based on the load flow results, and set $J_{last} = J(i, j, k, l)$.
 - Step 3:** Identify the busbar with the highest voltage unbalance $n_{VUF_{max}}$ and, then identify the busbars within the radius of k_n busbars from the busbar with highest unbalance $n_{VUF_{max}}$ to form the highest unbalance region, \mathbb{H}_{VU} .
 - Step 4:** Randomly change the phase combination of PV systems in the highest unbalance region \mathbb{H}_{VU} to find a phase combination with lower-cost value compared to J_{last} .
 - Step 5:** If a suitable phase combination is identified within N_r steps, then use that phase combination as the updated phase combination, $x^i(j + 1, k, l)$.
 - Step 6:** Else, $x^i(j + 1, k, l) = x^i(j, k, l)$.
-

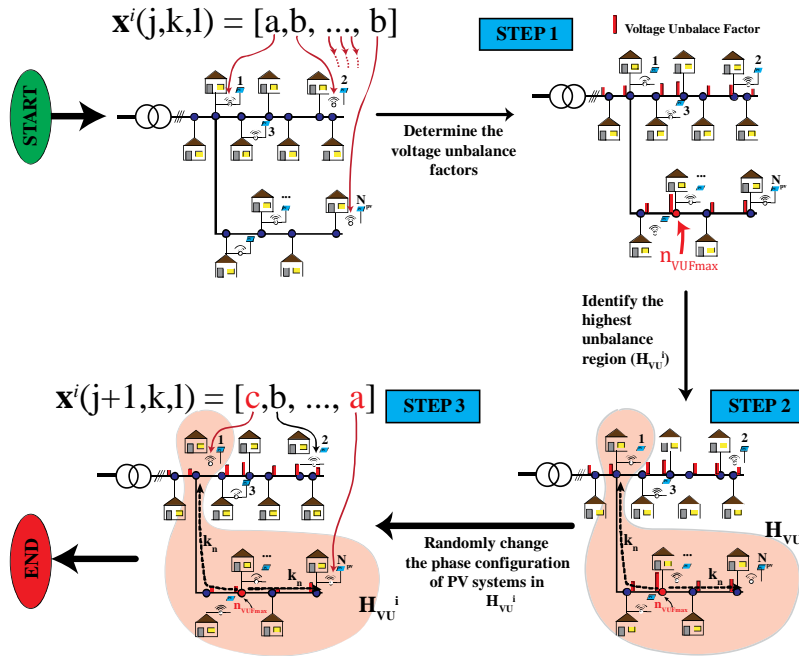


Figure 5: Proposed D-Chemotaxis procedure

4.2.2. Discrete Reproduction (D-Reproduction)

In D-Reproduction, the PV configuration vector having the highest cumulative cost (i.e. worst PV configuration) is eventually replaced by the PV configuration vector with the least cumulative cost (i.e. best PV configuration). The cumulative cost of the i -th PV configuration vector (J_C^i) for a given k and l was calculated from,

$$J_C^i = \sum_{j=1}^{N_c+1} J(i, j, k, l) \quad (10)$$

The pseudocode of the D-Reproduction step is given in Algorithm 2.

Algorithm 2: D-Reproduction

- Step 1:** Determine the cumulative cost J_C of all the PV configuration vectors for given k and l from Equation (10).
 - Step 2:** Replace the phase combination of the PV configuration vector having the highest cumulative cost by the phase combination of the PV configuration vector having the least cumulative cost.
-

4.2.3. Discrete Elimination Dispersal (D-Elimination Dispersal)

In D-Elimination Dispersal, some PV configuration vectors are randomly liquidated (eliminated) with a very small probability P_{ed} while the new replacements are randomly initialized over the search space. The D-Elimination Dispersal operator helps PV combinations that are trapped in local minima to escape.

The pseudocode of the D-Elimination Dispersal step is given in Algorithm 3.

Algorithm 3: D-Elimination Dispersal

- Step 1:** For all PV configuration vectors (i.e. for $i = 1, 2, 3, \dots, S$) repeat the following steps to perform D-Elimination dispersal.
 - Step 2:** Generate a Random Number between 0 and 1: $RN^i = rand(0, 1)$.
 - Step 3:** If $RN^i \leq P_{ed}$, Replace the phase combination in i -th PV configuration vector by a random phase combination.
 - Step 4:** Else, proceed to Step 2 for the next PV configuration vector ($i = i + 1$).
-

4.3. Initialization of PV configuration vectors

The BFOA is a population-based optimization algorithm. Hence, the quality of the optimal solution and the time to convergence heavily depend on the initial population (in this paper the initial population is also referred to as the set of PV configuration initializers to add more contextual flavor). In most of the situations, the initial population is randomly selected from the solution

space. However, it has been noted that random initialization is not an effective way to initialize the PV configuration initializers, especially when more contextual information is available to better optimize the selection of the initial points. Therefore, a novel initialization method was introduced to identify the suitable phase combinations for PV configuration initializers. A performance comparison is added in the results and discussion to highlight the effectiveness of the proposed initialization technique.

The proposed initialization method determines the initial phase combinations for the PV configuration initializers in such a way that those initial phase combinations have a smaller active power mismatch (see algorithm 4, step 4) at the secondary side of the MV-LV transformer. The suitable phase combinations with smaller active power mismatch were selected from the brute force checking strategy where the active power mismatch for the whole solution space is computed to identify the phase combinations that have smaller active power mismatch.

However, it was observed that for an LVDG network having a large number of grid-connected PV systems, the brute force searching takes a longer time to find a set of suitable phase combinations with smaller active power mismatch because the algorithm needs to go through the entire solution space to identify the phase combinations that have smaller active power mismatch. For an example, let us consider the network used for the simulation (see Figure 9) which has 26 number of grid-connected PV systems. For this network, the initialization algorithm should go through approximately $3^{26} \approx 2.54$ trillion possible phase combinations (solutions) to identify the best phase combinations having smaller active power mismatch if the partitioning of the network is not considered. This not only leads to a longer execution time but also requires massive computer memory to execute the algorithm.

As a solution to the above problem, the network was partitioned into smaller zones/regions (R_1, R_2, R_3, \dots) which have about 2-6 nearby grid-connected PV systems, which are then utilized to identify phase combinations with smaller active power mismatch for each zone (see Figure 9). In this way, the possible phase combinations (solutions) of each zone is in the order of hundreds ($3^6 = 729$) and the initialization can be done very fast according to the algorithm outlined in Algorithm 4. In addition, this method does not require a large memory to execute and can also be executed in parallel for all the zones at the same time to make the initialization even faster. In other words, a regional minimization is performed to facilitate global optimization. The proposed initialization process is graphically illustrated in Figure 6 and the pseudocode is given in Algorithm 4.

Algorithm 4: Initialization of PV configuration initializers

- Step 1:** Collect active power consumption of loads and the active power generation by PV systems through smart meters.
- Step 2:** Partition the large network into smaller regions ($R_1, R_2, R_3, \dots, R_r$).

- Step 3:** Identify the solution space (i.e. all possible phase combinations) for each region.
 Note: For a region having w number of grid-connected PV systems, there are 3^w possible phase combinations in the solution space.
- Step 4:** *Execute in parallel for $R_1, R_2, R_3, \dots, R_r$:*
- 1) Calculate the active power mismatch for each phase combination in the solution space. The active power mismatch is quantified by the standard deviation of the three-phase active power in that region.
 - 2) Identify $k_R (= 4)$ phase combinations having a smallest active power mismatch among the all possible phase combinations.
- Step 5:** Randomly combine the identified phase combinations for each region to form the initial phase combinations for PV configuration initializers.

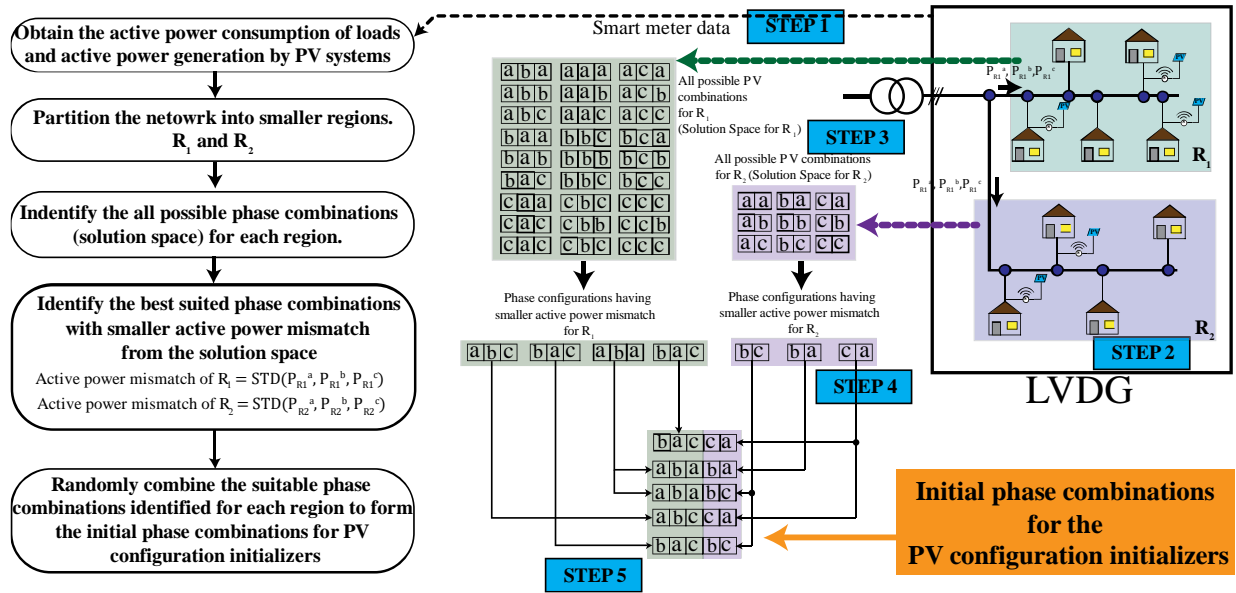


Figure 6: Generation of initial phase combinations for PV configuration initializers based on active power balancing technique for a large distribution network.

4.4. Implementation of DBFOA

4.4.1. The complete structure of the proposed DBFOA

The complete structure of the proposed DBFOA is shown in Figure 7.

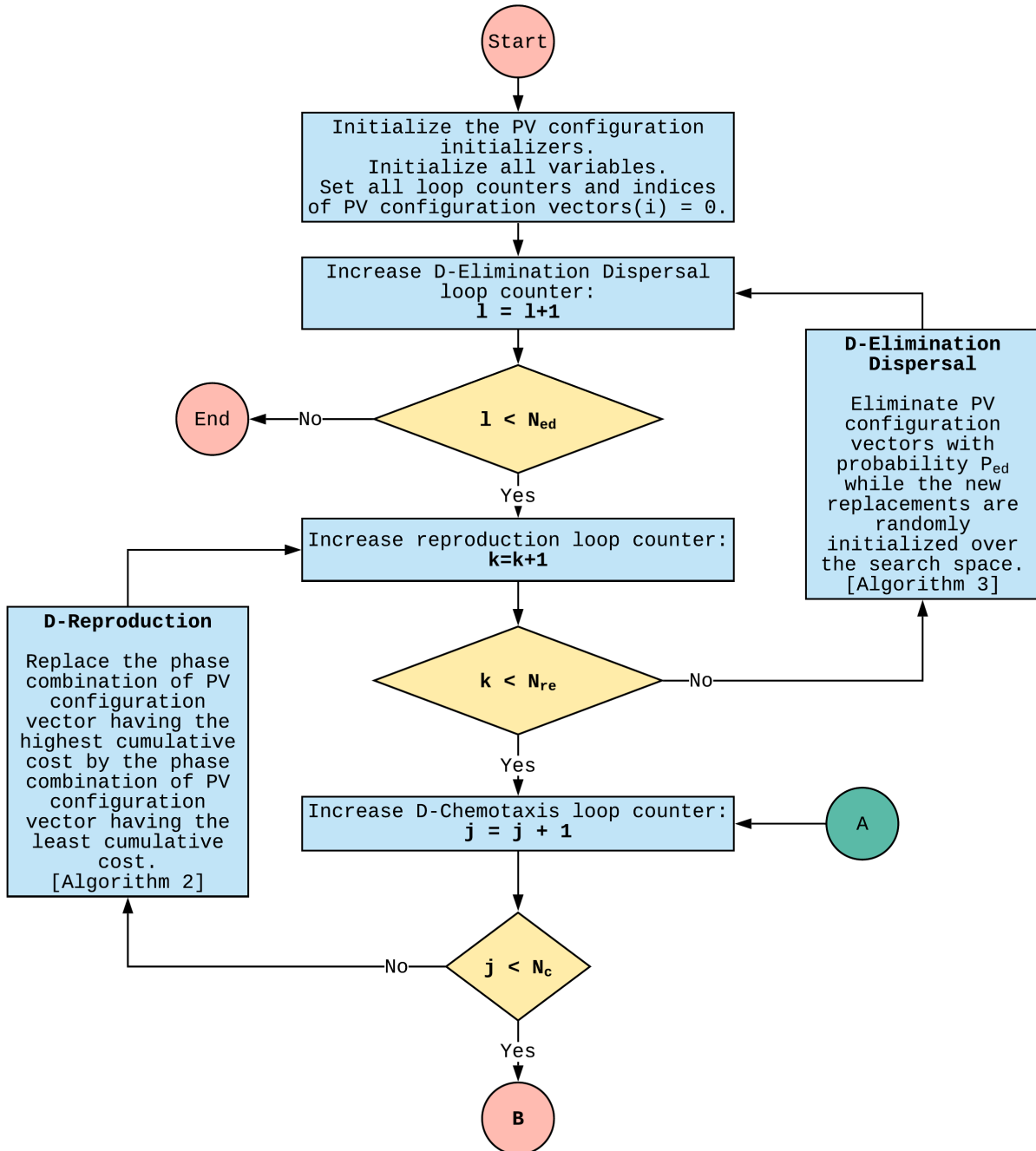


Figure 7: Continued.

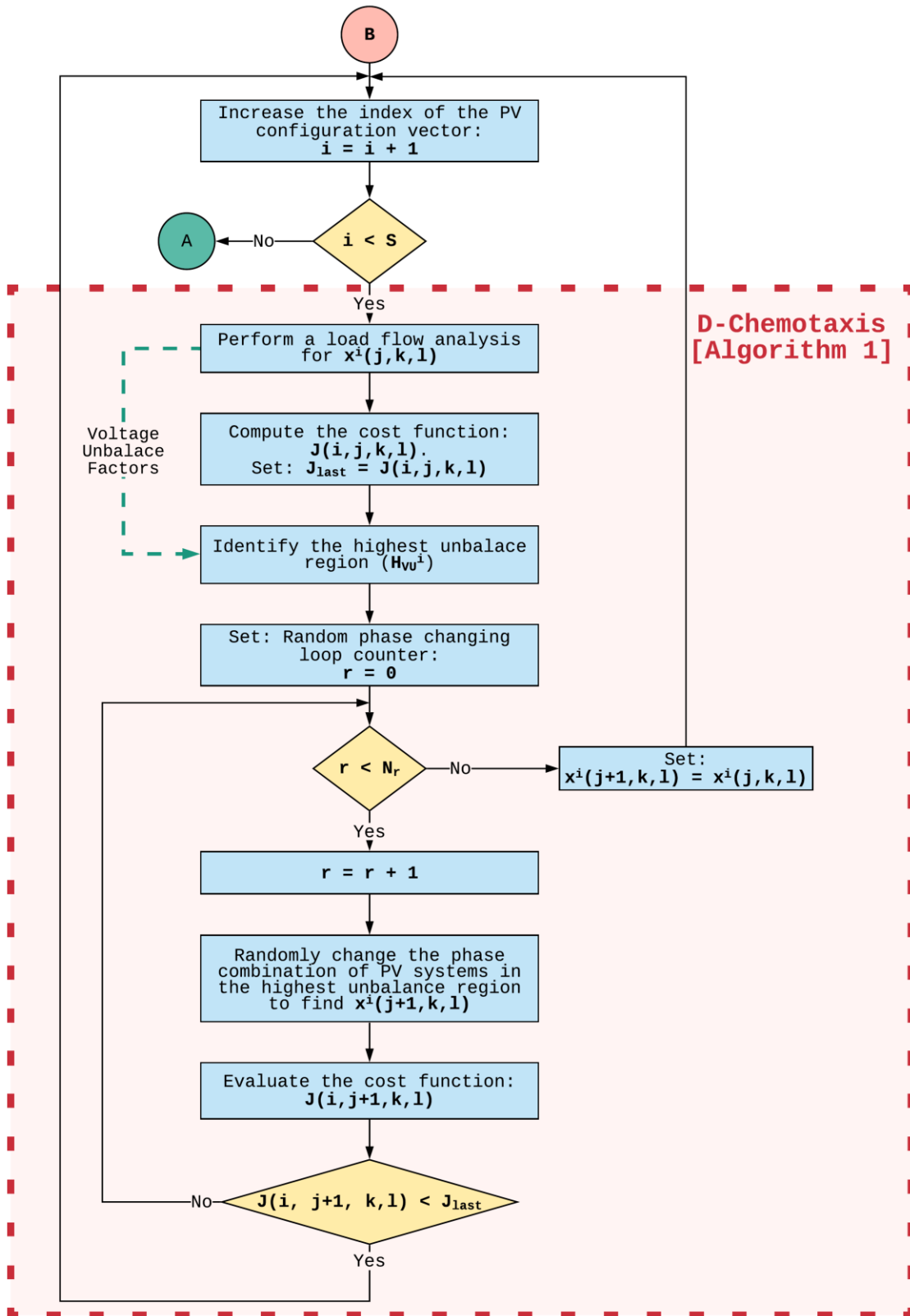


Figure 7: The complete structure of the proposed DBFOA

4.4.2. Pseudocode of DBFOA

The pseudocode of the proposed DBFOA applied to reduce overall unbalance of a network is given in Algorithm 5.

Algorithm 5: The proposed DBFOA

- Step 1:** Initialize all the PV configuration initializers - \mathbf{x}^i (use Algorithm 4).
Initialize of the following parameters:
- S : The number of PV configuration initializers.
 - N_c : The maximum number of D-Chemotaxis is performed.
 - N_s : The Maximum number of times random phase changing is performed.
 - N_{re} : The maximum number of times D-Reproduction is performed.
 - P_{ed} : The probability that each PV configuration vectors are eliminated.
- Set all loop counters to zero.**
- Incremental counter for D-Elimination dispersal step (l) = 0.
 - Incremental counter for D-Reproduction step (k) = 0.
 - Incremental counter for D-Chemotaxis step (j) = 0.
 - Index of the PV configuration vectors (i) = 0.
- Step 2:** D-Elimination Dispersal loop: $l = l + 1$.
- Step 3:** D-Reproduction loop: $k = k + 1$.
- Step 4:** **D-Chemotaxis loop**, $j = j + 1$. [Algorithm 1]
- A.** For $i = 1, 2, \dots, S$, execute a D-Chemotaxis step for i -th PV configuration vector as follows.
 - B.** Perform a load flow analysis for the phase combination in i -th PV configuration vector - $\mathbf{x}^i(j, k, l)$ to obtain three-phase voltages and voltage unbalance factors.
 - C.** Evaluate the cost function $J(i, j, k, l)$.
 - D.** Let $J_{last} = J(i, j, k, l)$ so that the PV configuration vector having a lower cost could be identified.
 - E.** Identify the highest voltage unbalance region \mathbb{H}_{VU}^i corresponding to phase combination $\mathbf{x}^i(j, k, l)$ from the voltage unbalance factors obtained in **Step 4 B**.
 - F.** Set: random phase changing loop counter to zero, $r = 0$.
 - G.** **While** $r < N_r$,
 - i. Increment the random phase changing loop counter: $r = r + 1$.
 - ii. Randomly change the phase combination of the PV systems in the highest unbalance region to determine the new phase combination of i -th PV configuration vector $\mathbf{x}^i(j + 1, k, l)$.

- iii. Evaluate the cost function $J(i, j + 1, k, l)$ corresponding to the phase combination $\mathbf{x}^i(j + 1, k, l)$.
- iv. **If:** $J(i, j + 1, k, l) < J_{last}$,
Go to the next PV configuration vector ($i = i + 1$) (i.e. Go to **Step 4 B.** to process the next PV configuration vector).
- v. **Else:**
Go to **Step 4 G.**

H. End of while.

Couldn't find a phase combination better than $\mathbf{x}^i(j, k, l)$.

Set $\mathbf{x}^i(j + 1, k, l) = \mathbf{x}^i(j, k, l)$.

Go to the next PV configuration vector ($i = i + 1$) (i.e. Go to **Step 4 B.** to process the next PV configuration vector).

Step 5: **If,** $j < N_c$ go to **Step 4** ($j = j + 1$). In this case, continue D-Chemotaxis.
Else, go to **Step 6.**

Step 6: D-Reproduction [Algorithm 2]:

- A. For the given k and l , and for each $i = 1, 2, \dots, S$ evaluate the cumulative cost of i -th PV configuration vector as follows:

$$J_C^i = \sum_{j=1}^{N_c+1} J(i, j, k, l) \quad (11)$$

- B. Replace the phase combination of the PV configuration vector having the highest cumulative cost by the phase combination of the PV configuration vector having the least cumulative cost.

Step 7: **If** $k < N_{re}$, go to **Step 3** ($k = k + 1$). We have not reached the number of specified D-reproduction steps, so we start the next generation of the D-Chemotaxis loop.

Else, go to **Step 8.**

Step 8: D-Elimination Dispersal [Algorithm 3]:

- **For** $i = 1, 2, \dots, S$, eliminate PV configuration vectors with probability P_{ed} while the new replacements are randomly initialized over the search space.

Step 9: **If,** $l < N_{ed}$, go to *Step 2* ($l = l + 1$);

Else, End.

4.4.3. Parameters of DBFOA

The parameter values used in the proposed DBFOA are given in Table 3. The number of PV configuration initializers (S), and the values for N_c , N_r , N_{re} , and N_{ed} were selected by considering the convergence speed of the DBFOA and the values used in the previous studies [55,57,58]. The elimination-dispersal probability - P_{ed} and the radius of the highest unbalance region - k_n were selected to maximize the convergence speed of DBFOA by executing the algorithm for a possible range of values for P_{ed} and k_n .

Table 3: Parameter values used for the proposed DBFOA

Parameter	Value
Number of PV configuration initializers (S)	10
Maximum number of D-Chemotaxis steps (N_c)	5
Maximum number of random phase changing steps (N_r)	5
Maximum number of D-Reproduction steps (N_{re})	5
Maximum number of D-Elimination steps (N_{ed})	5
Elimination & dispersal probability (P_{ed})	0.2
The radius of the highest voltage unbalance region - $\mathbb{H}_{VU}(k_n)$	3
The maximum limit for phase voltage magnitudes (V_{max})	1.06 pu
The minimum limit for phase voltage magnitudes (V_{min})	0.94 pu
The maximum limit for voltage unbalance factors (VUF_{max})	1%
Number of grid-connected PV systems in the network (N_{pv})	26
Number of busbars in the network (N)	63

5. Test network

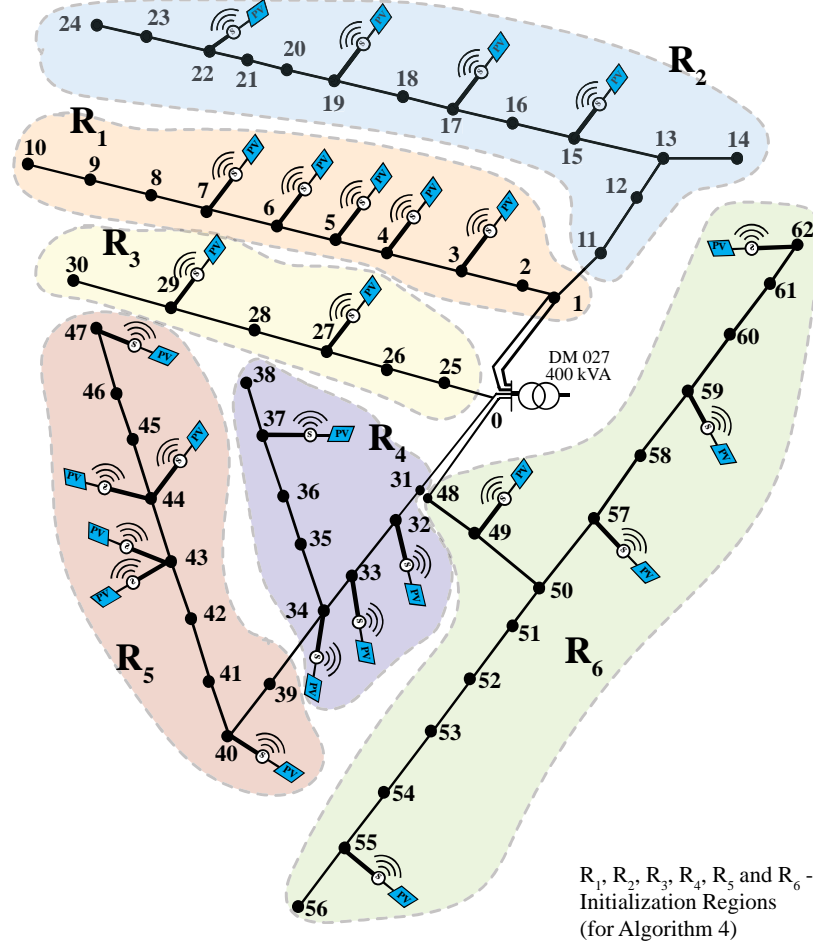


Figure 8: Single line diagram of the test LVDG network (Lotus Grove, Sri Lanka) used for the simulations.

The network topology with 63 busbars as shown in Figure 8 was used for the simulations. The number 0 node is the root node and connected to the secondary side of the MV-LV transformer. The rated capacity of the transformer is 400 kVA and the input/output voltage rating is 11 kV/415 V. The solid lines in Figure 8 represent the three-phase feeders with three-phase or single-phase loads and PV systems connected. The per length impedance matrix of the feeder line is given in Table 4.

Table 4: Impedance matrix (Z^{abcn}) per km for the overhead cable (ABC 70) in the network.

	Phase a	Phase b	Phase c	neutral
Phase a	$0.4918 + 0.7888i$	$0.0486 + 0.6292i$	$0.0487 + 0.6701i$	$0.0486 + 0.7000i$
Phase b	$0.0486 + 0.6292i$	$0.4918 + 0.7888i$	$0.0487 + 0.6405i$	$0.0486 + 0.6490i$
Phase c	$0.0487 + 0.6701i$	$0.0487 + 0.6405i$	$0.4918 + 0.7888i$	$0.0487 + 0.7080i$
neutral	$0.0486 + 0.7000i$	$0.0486 + 0.6490i$	$0.0487 + 0.7080i$	$0.6790 + 0.7910i$

There are 26 grid-connected single-phase PV systems and 92 single-phase or three-phase loads. The capacity of PV systems, their locations, and their default phase configuration are given in Table 5 and the daily operation curve (hourly generation profile) of PV systems is shown in Figure 9-(a).

Table 5: The details of the grid-connected single-phase PV systems connected to the network

PV No.	Connected busbar	Initial phase configuration (Fixed phase)	Capacity (P_{max})/ kW
PV1	3	a	2.40
PV2	4	b	7.20
PV3	5	a	4.80
PV4	6	c	2.40
PV5	7	a	6.00
PV6	15	a	5.04
PV7	17	b	5.04
PV8	19	a	2.40
PV9	22	c	8.20
PV10	27	a	4.80
PV11	29	c	6.48
PV12	32	a	6.00
PV13	33	b	3.96
PV14	34	a	6.00
PV15	37	b	3.12
PV16	40	c	4.20
PV17	43	c	6.00
PV18	43	b	8.2
PV19	44	c	6.36
PV20	44	b	5.76
PV21	47	a	8.28
PV22	49	a	5.16
PV23	55	c	8.40
PV23	57	b	2.20
PV25	59	a	4.80
PV26	62	c	7.20

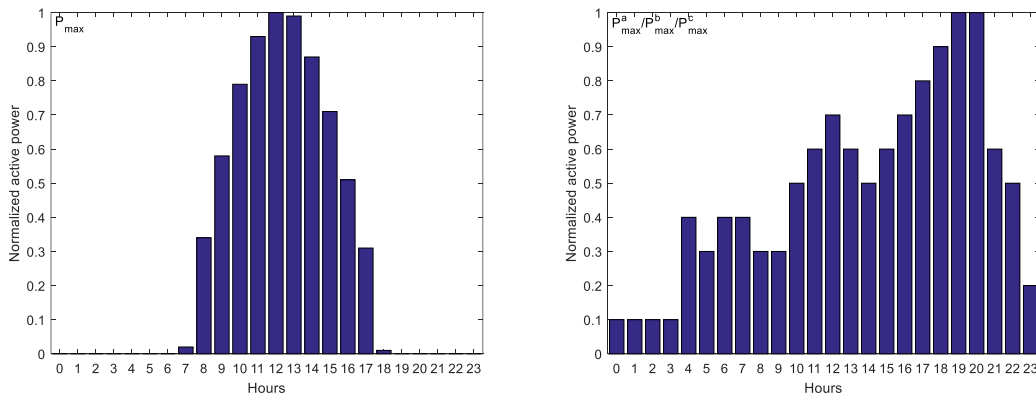


Figure 9: (a) Hourly generation profile of PV systems (b) hourly load profile for single-phase/ three-phase loads.

Moreover, the network shown in Figure 8 consists of 92 single-phase and three-phase loads. The maximum capacity of loads and their power factor values at each busbar are given in Table 6, and the hourly load profile of loads is shown in Figure 9-(b).

Table 6: The capacity of loads and power factor values at each busbar

Busbar	Active power/ (kW)			pf	Busbar	Active power/ (kW)			pf
	P_{max}^a (kW)	P_{max}^b (kW)	P_{max}^{ac} (kW)			P_{max}^a (kW)	P_{max}^b (kW)	P_{max}^c (kW)	
1	2.19	0.55	1.85	0.981	35	0.85	0.88	0.75	0.949
1	1.28	0.46	0.55	0.991	36	0.67	1.45	1.27	0.945
1	2.43	0.28	1.88	0.913	37	0.79	0.66	1.24	0.965
2	2.33	0.26	1.50	0.991	37	1.91	1.14	1.63	0.971
3	0.19	0.45	0.34	0.963	38	1.97	1.55	1.27	0.975
3	0.12	0.69	0.68	0.910	41	1.72	1.05	2.01	0.928
4	0.33	0.58	0.17	0.928	41	1.35	1.15	1.39	0.968
4	0.48	0.52	1.08	0.955	42	0.47	0.60	0.32	0.966
5	0.54	1.36	0.69	0.996	42	1.27	1.50	1.11	0.916
5	1.43	1.43	1.33	0.996	43	1.97	0.30	2.12	0.912
6	1.53	2.22	0.64	0.916	43	1.27	1.04	0.87	0.950
6	1.04	0.78	0.27	0.997	44	0.98	0.25	1.86	0.996
7	0.24	0.25	0.29	0.996	44	1.72	0.65	0.41	0.934
7	0.56	1.24	0.79	0.949	45	1.06	1.71	1.81	0.959
8	0.54	1.09	2.46	0.980	45	0.70	0.76	1.02	0.922
8	1.76	0.42	0.90	0.914	45	0.41	2.49	1.99	0.975
9	1.03	2.79	0.86	0.942	45	0.69	1.43	1.07	0.926
9	1.18	0.51	0.99	0.992	46	0.46	0.15	0.18	0.951
10	0.91	4.05	0.06	0.979	46	2.11	1.02	1.85	0.970
13	1.39	1.45	0.74	0.996	46	1.01	1.88	1.50	0.989
14	0.16	0.38	0.15	0.966	47	1.22	1.05	1.22	0.996
15	4.93	1.57	0.14	0.904	47	2.59	1.19	1.10	0.955
15	1.39	2.17	0.32	0.985	47	1.39	2.61	0.29	0.914
16	0.96	0.90	0.53	0.993	50	2.03	0.89	1.17	0.915
16	1.44	2.95	0.50	0.968	51	2.05	0.87	1.86	0.926
17	0.77	0.69	0.72	0.976	51	0.48	0.17	0.54	0.984
17	0.92	1.05	0.82	0.974	52	0.42	0.43	0.24	0.925
18	0.21	0.74	1.13	0.939	52	1.20	1.57	1.52	0.981
18	1.03	1.18	1.88	0.966	53	0.59	0.29	0.81	0.924
19	0.34	2.01	1.63	0.917	53	1.76	2.61	0.42	0.993
19	1.51	1.04	1.44	0.971	54	0.78	1.12	0.89	0.935
20	1.14	1.03	0.21	0.903	54	3.42	1.45	0.18	0.920
21	0.73	0.58	0.97	0.928	55	0.16	0.04	0.19	0.925
22	1.37	1.89	0.52	0.905	55	0.13	0.09	0.06	0.962
22	1.32	1.94	1.02	0.910	56	2.36	1.45	0.97	0.947
23	1.28	1.45	1.56	0.982	57	0.76	1.03	1.79	0.935
23	0.40	0.27	0.21	0.969	57	1.56	0.83	0.99	0.983
24	0.26	0.07	0.26	0.932	58	1.69	0.33	1.56	0.959
25	0.90	1.99	0.69	0.995	58	1.32	1.37	1.60	0.955
26	2.04	1.80	0.84	0.903	59	0.98	1.85	3.82	0.992
27	4.62	0.12	0.30	0.944	59	0.95	0.68	0.75	0.929
28	0.52	2.18	1.98	0.938	60	0.99	1.35	1.45	0.976
29	0.27	0.59	0.42	0.977	60	0.74	1.04	0.81	0.975
30	1.35	2.42	0.72	0.980	61	0.98	1.85	3.82	0.938
35	2.25	0.92	0.82	0.919	62	0.95	0.68	0.75	0.957

6. Results and Discussion

6.1. Convergence characteristics of the proposed DBFOA

6.1.1. The effect of D-Chemotaxis

This section demonstrates the effectiveness of the D-Chemotaxis procedure utilized in DBFOA. The proposed D-Chemotaxis is specially designed for the PV re-phasing problem as opposed to merely directly adopting it from classical chemotaxis. The proposed D-Chemotaxis identifies the region around the busbar with the highest unbalance (\mathbb{H}_{VU}) and then, only the phase combination of grid-connected PV systems in that region are randomly changed to find the optimal solution iteratively. However, in classical chemotaxis, a fixed number of PV systems are randomly selected from the network and then, the phase configurations of those PV systems are randomly changed. This random selection of PV systems in classical chemotaxis may result in the formation of much higher unbalance levels in the network, thus, ultimately resulting in slower convergence.

Since the increase in voltage unbalance levels of a particular region of a network is mainly due to the mismatch of active and reactive power levels in the same region, the proposed D-chemotaxis step randomly changes the phase configuration of PV systems in the highest unbalance region iteratively. This could lead to a dramatic increase in the convergence speed of the DBFOA as shown in Figure 10. According to the results, the proposed D-chemotaxis step in the DBFOA resulted in faster convergence of the algorithm when compared to the classical chemotaxis under the same conditions (same initial population, same values for parameters, etc.). Also, the proposed chemotaxis step causes the optimal solution to settle in a place with lower cost value as opposed to classical chemotaxis where final settling cost is much higher as Figure 10 depicts.

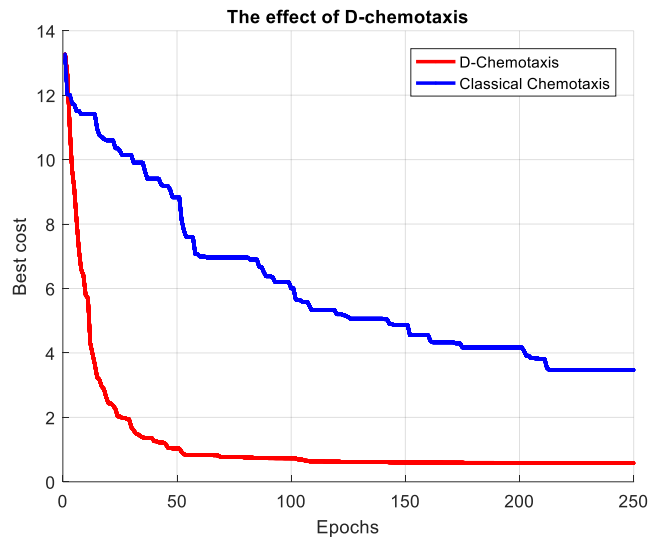


Figure 10: The effect of D-chemotaxis on the convergence of DBFOA.

6.1.2. Effect of the initialization of the PV configuration initializers

As described in section 4.3, an active power balancing approach was introduced to find initial phase combinations for the PV configuration initializers as opposed to the random initialization of the classical technique. Figure 11 depicts the convergence properties of the DBFOA under two cases: (1). The PV configuration initializers were initialized based on the active power balancing technique and (2). The PV configuration initializers were randomly initialized. According to the results, the starting cost of DBFOA under the proposed power balancing initialization is approximately 83% lower than the random initialization. This implies that the active power balancing technique was able to generate phase combinations that are closer to the optimal phase combination. Ultimately, the DBFOA with the proposed initialization technique converged to the optimal solution with fewer iterations compared to the random initialization.

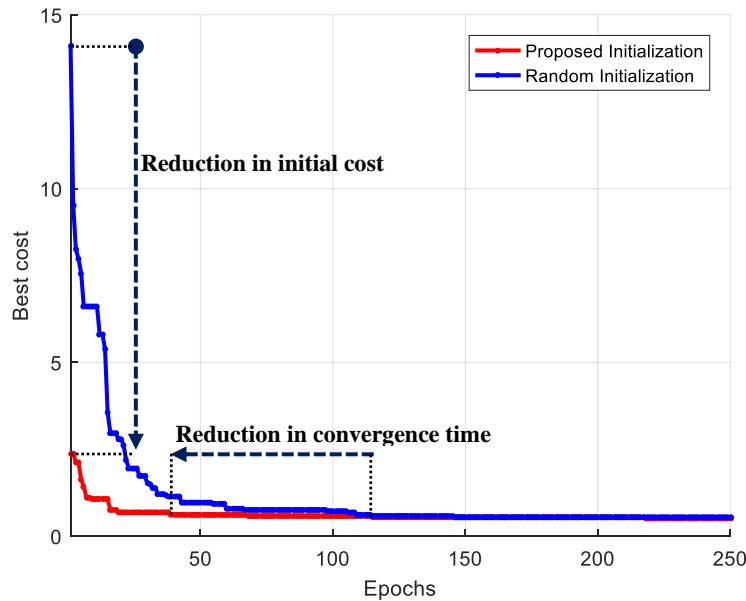


Figure 11: Convergence of the DBFOA for proposed and random initialization methods.

6.2. Effects of PV re-phasing

This section demonstrates the effect of PV re-phasing on voltage unbalance and phase voltage magnitudes of residential distribution grid with high penetration of solar power. The proposed PV re-phasing algorithm was implemented on the real distribution network shown in Figure 8. The variations of loads and PV power generation throughout the day were considered in the simulations by utilizing hourly load and PV generation profiles shown in Figure 9.

The goal of PV re-phasing is to reduce overall voltage unbalance (\overline{VUF}) of the network by dynamically changing the phase configuration of rooftop solar systems in the network. Figure 12 and 13 clearly illustrate the effect of PV re-phasing on the overall voltage unbalance and phase voltages, respectively. According to Figure 12, significantly high voltage unbalances are observed during the daytime when PV systems have a fixed phase configuration. Whereas the dynamic PV re-phasing significantly reduces the overall voltage unbalance of the network (mean unbalance is

below 1 %) especially during the period from 8 am to 5 pm, where high PV penetration is present. In addition, Table 7 provides the optimal phase configuration of PV systems that are determined from the proposed DBFOA from 6 am to 7 pm. The colored cells in Table 7 belong to the phases of PV systems that are not changed in the subsequent hour. Since not each rooftop PV system is subjected to PV re-phasing at each hour, SCADA needs to send the PV re-phasing commands only for the rooftop solar systems that are required to re-phase in the next PV-rephasing operation. Moreover, the proposed algorithm can be improved to minimize the number of PV re-phasing operations that each rooftop PV system undergoes throughout the day by modifying the cost function of the optimization algorithm. Finally, these results confirm that the proposed re-phasing strategy is successful in reducing the voltage unbalance levels of domestic distribution grids that have many grid-connected rooftop PV systems, while simultaneously maintaining the phase voltages within their acceptable limits.

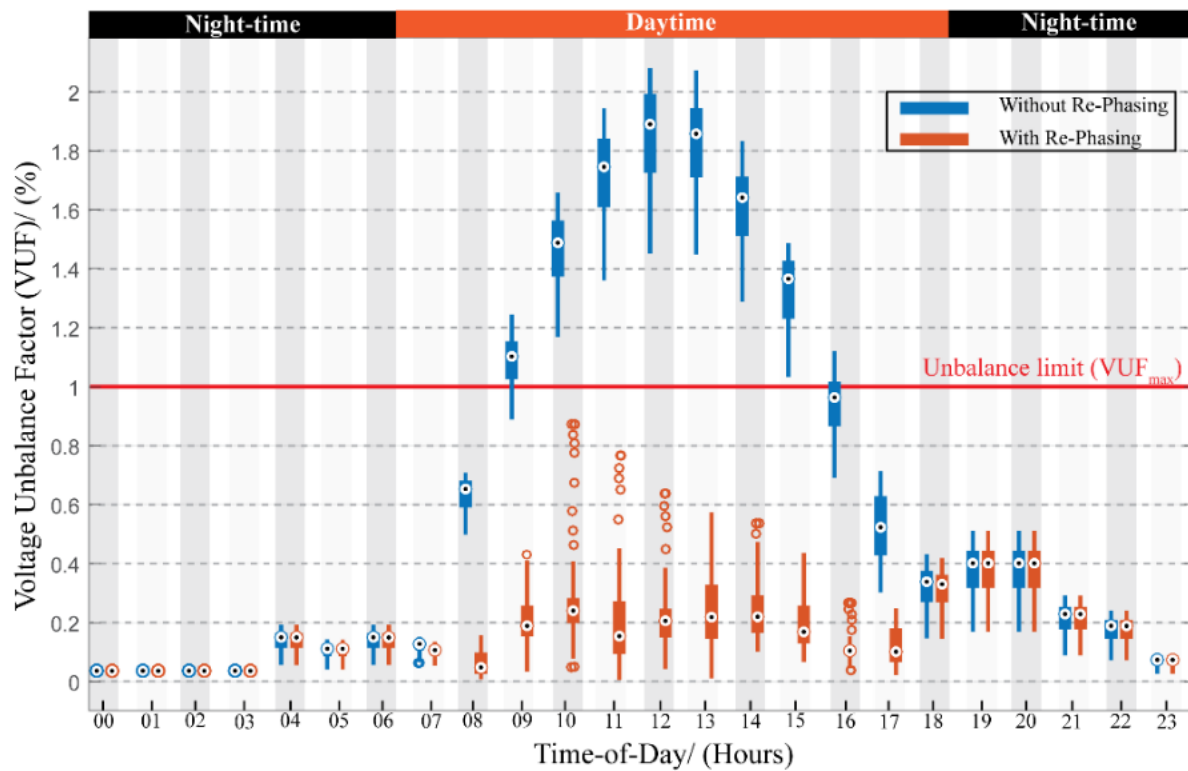
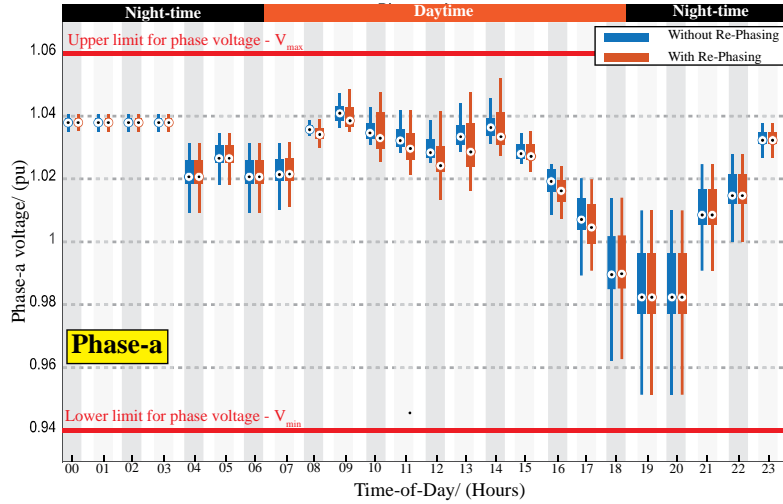
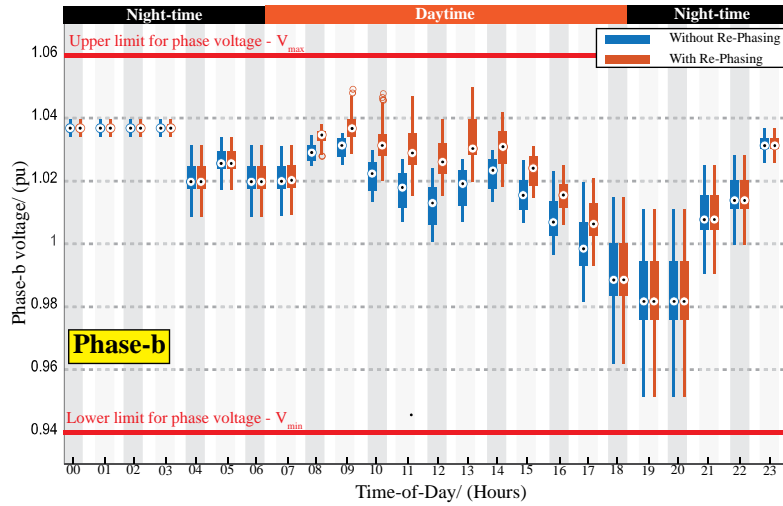


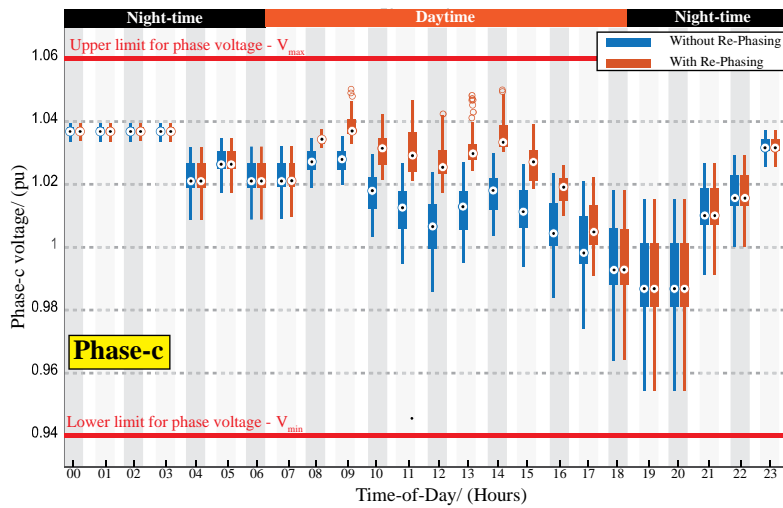
Figure 12: Distribution of voltage unbalance values of the network throughout the day for ‘with’ and ‘without’ PV re-phasing.



(a)



(b)



(c)

Figure 13: Evolution of (a) phase-a, (b) phase-b, and (c) phase-c voltage of the network throughout the day for 'with' and 'without' PV re-phasing.

Table 7: Hourly phase configurations of rooftop PV systems determined by the proposed DBFOA. The colored cells in the table represent the phase configuration of rooftop solar systems that are not changed in the subsequent hour.

Time	Hourly phase configuration of rooftop PV systems (a = Phase a, b = Phase b, and c= Phase c)																									
	1	2	3	4	5	6	7	8	9	10	11	12	13	14	15	16	17	18	19	20	21	22	23	24	25	26
6 - 7 am	b	b	a	a	c	b	c	c	b	b	a	b	c	a	a	a	a	a	a	a	a	b	a	b	b	a
7 - 8 am	a	a	a	b	a	a	b	a	a	c	a	c	a	a	c	b	a	a	a	a	a	a	b	b	a	a
8 - 9 am	a	a	a	a	a	a	a	b	b	a	a	a	b	b	a	a	a	a	a	a	b	b	b	a	a	a
9 - 10 am	a	c	a	b	b	a	a	c	b	c	c	b	b	a	b	c	a	a	a	a	a	a	a	a	b	a
10 - 11 am	c	a	c	a	a	c	a	a	b	a	b	c	a	a	c	b	b	a	b	c	b	a	a	a	a	b
11 - 12 am	a	a	a	a	b	a	a	a	a	c	c	b	c	b	b	c	a	b	a	a	a	a	a	a	a	a
12 - 1 pm	b	a	a	a	a	a	a	c	c	a	b	a	a	a	b	a	a	a	a	b	a	b	a	a	b	b
1 - 2 pm	a	b	a	a	a	a	a	a	b	b	c	b	b	b	a	b	a	a	b	a	c	b	a	a	a	a
2 - 3 pm	a	a	b	a	a	a	a	a	a	c	a	c	a	a	c	a	a	a	a	a	b	a	c	b	a	a
3 - 4 pm	a	a	a	a	a	a	a	b	b	b	a	b	b	b	b	b	a	a	a	a	b	b	a	a	a	a
4 - 5 pm	a	a	a	a	a	a	a	c	b	b	c	b	b	b	a	c	a	a	a	a	b	b	a	a	a	a
5 - 6 pm	a	a	a	a	b	b	a	a	a	b	a	a	c	c	b	b	a	b	a	a	b	a	a	a	a	a
6 - 7 pm	a	a	a	a	a	a	a	a	b	a	b	b	a	b	a	a	a	a	a	a	a	b	a	a	a	a
7 - 8 pm	a	b	a	b	a	a	b	b	c	b	b	b	c	c	c	c	a	a	b	a	c	c	a	a	b	b

Since the proposed PV re-phasing technique can maintain the voltage imbalances of the network well below the 1% threshold during the daytime while keeping the phase voltages within their acceptable voltage range, utility providers can allow additional rooftop solar systems into the network. In order to get a clear idea about the amount of additional renewable energy capacity facilitated by the PV re-phasing operation, simulations were performed by adding new rooftop solar systems (on top of existing 140.4 kW of solar PV as specified by Table 5) to the existing network. For each addition of a new rooftop solar system, 20 Monte-Carlo simulations were performed by randomly changing its connection point in the LV network to ensure an unbiased and fair simulation. For this study, the capacity of each new rooftop solar system to be connected to the existing LV network is considered to be 5.4 kW that corresponds to the average capacity of a rooftop PV system in the existing network. The maximum voltage unbalances and maximum phase voltage values of the network recorded for “with” and “without” re-phasing are depicted in Figure 14.

According to Figure 14-(c), the maximum voltage unbalance of the network is well below the 1% threshold for the proposed PV re-phasing technique even under the integration of new rooftop solar systems up to a total capacity of 302.4 kW. In contrast, as can be seen from Figure 14-(a), the maximum voltage unbalance values of the network exceed the 1% threshold line for the fixed phase configuration. However, as depicted in Figure 14 – (b) and (d), the maximum voltage of the network gradually increases with the addition of new rooftop solar systems to the network. Due to this reason, rooftop solar systems with a total capacity of 248.4 kW can be safely integrated into the LV network without violating the statutory limits of both voltage unbalance and phase voltage magnitudes. This is about a 77% increase in the rooftop solar capacity of the network compared to the originally installed solar capacity (140.4 kW). Therefore, it is apparent that the proposed PV re-phasing strategy can completely overcome the voltage unbalance issue due to the installation of distributed energy sources in the LV and facilitate to install additional rooftop solar systems into the network.

In addition, it should be pointed out that the above conclusions are made under the assumption that the voltage unbalance should be kept below 1%, and the phase voltage can vary between 0.94 pu and 1.06 pu ($\pm 6\%$ tolerance level). However, some countries/regions allow the phase voltage to vary within a larger range, such as 0.9 pu to 1.1 pu (that is, a $\pm 10\%$ tolerance level). Under this new voltage limit, the proposed PV re-phasing approach can increase the usable PV capacity of the network to more than *the capacity* obtained with a voltage tolerance of $\pm 6\%$. It can be seen from Figure 14-(d) that if the maximum allowable voltage level is 1.1 pu, solar PV totaling more than 302.4 kW can be safely integrated into the original network. That is approximately a 115% increase compared to the originally installed solar capacity (140.4 kW) of the network.

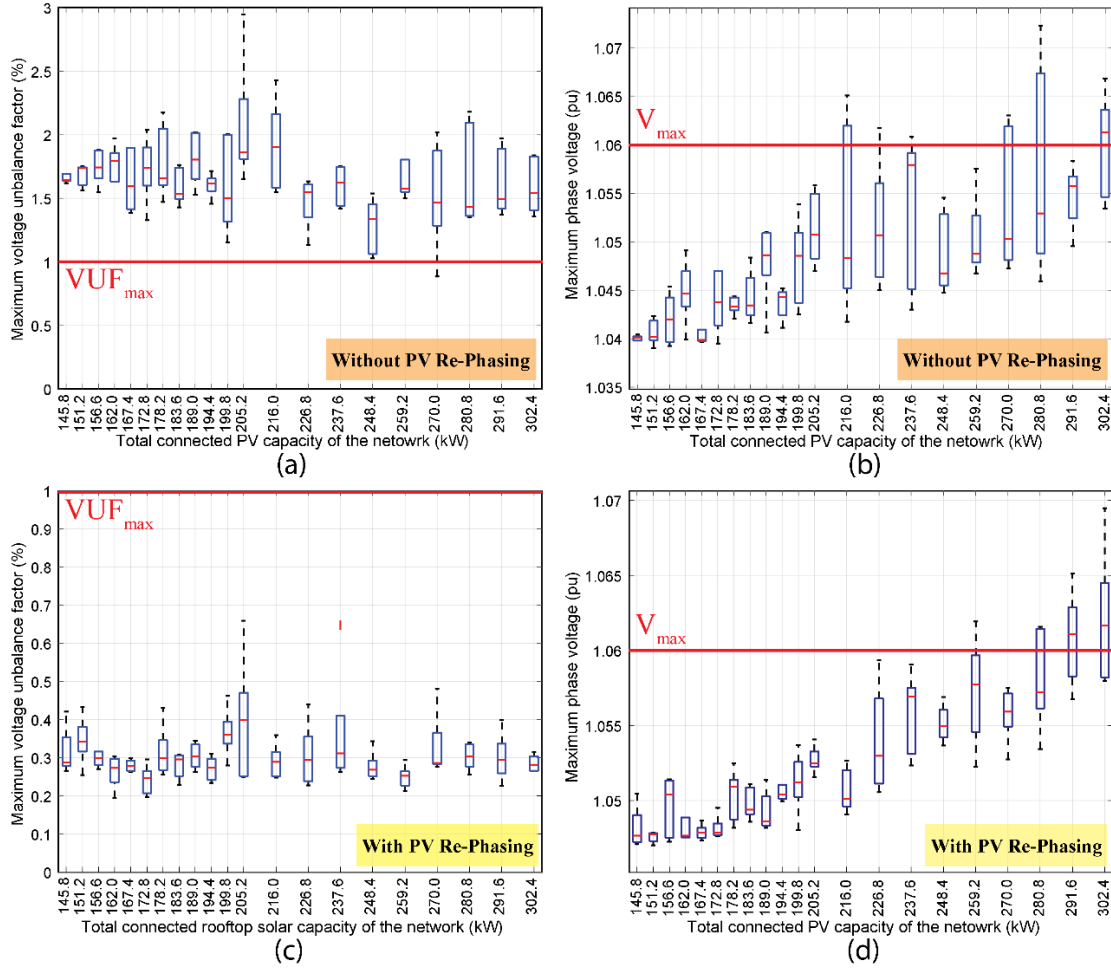


Figure 14: Variation of (a) maximum voltage unbalance and (b) maximum voltage unbalance with the total connected PV capacity of the LVDG network for “without” re-phasing. Variation of (c) maximum voltage unbalance and (d) phase voltage magnitude with the total connected rooftop solar capacity for “with” re-phasing.

6.3. Comparison of different optimization techniques

In order to predict the superiority of the proposed DBFOA, the convergence characteristics of the proposed DBFOA for the test system is compared with three other widely used optimization algorithms in power systems, namely, Discrete Genetic Algorithm (DGA), Shuffled Frog-Leaping Algorithm (SFLA) and Heuristic Search (HS), and the results are shown in Figure 15. The algorithms were written on Matlab[®] (version: R2016a) - Open DSS (version: 8.4.1.1) co-simulation environment and executed on a processor with Intel Core i7-7700HQ with 32 GB RAM running at 3.4 GHz. From the figure, it is clear that the DBFOA only takes 38 iterations to converge to the best solution. In addition to that, DBFOA shows a stable and quick convergence with a global searching capability to find the optimal phase configuration. Thereby, ensuring that the LVDG maintains strict power quality standards, even under heavy PV penetration in a near-real-time fashion.

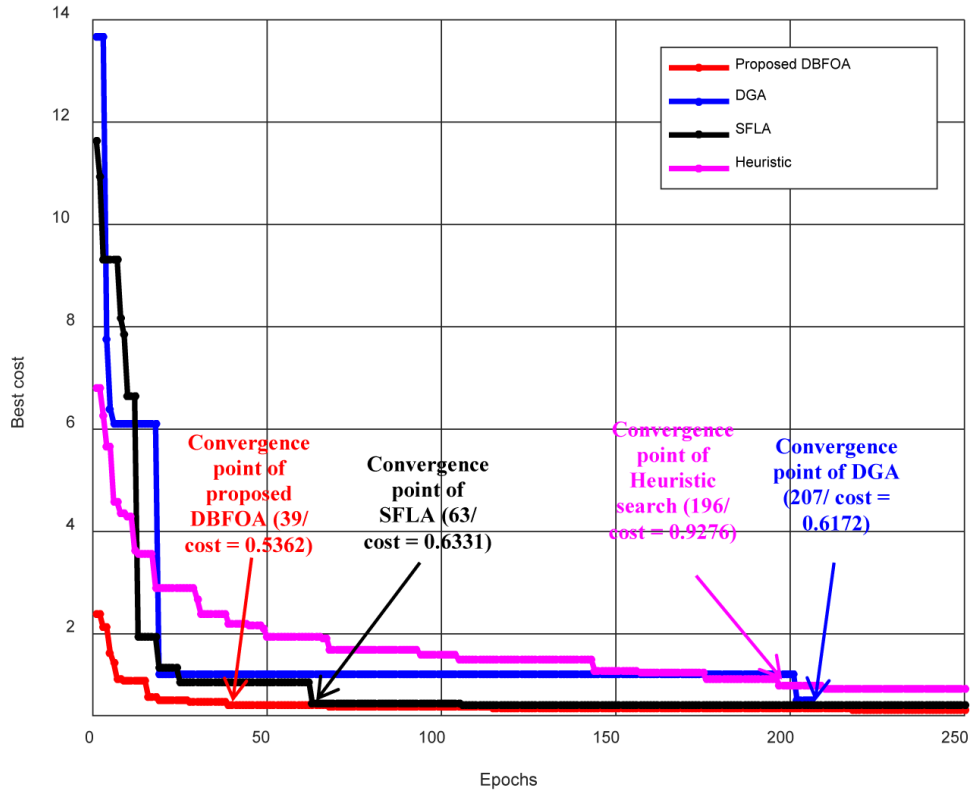


Figure 15: Performance comparison of proposed DBFOA with DGA, SFLA, and Heuristic search.

Table 8 shows the computational performance of the four algorithms. The average execution time of a single epoch for the three algorithms is almost the same. However, the proposed DBFOA converges to the optimal solution very fast compared to DGA, SFLA, and Heuristic Search.

Table 8: Computational efficiency of DBFOA, DGA, SFLA, and Heuristic search in terms of CPU time

Algorithm	Execution time/Epoch (s)	Time to convergence/ (s)	Cost after 250 epochs
Proposed DBFOA	0.888	33.744	0.5362
DGA	0.846	175.122	0.6172
SFLA	0.897	56.511	0.6331
Heuristic search	0.622	121.912	0.9276

7. Conclusion

In this paper, a novel method was introduced to mitigate the voltage unbalance in LV distribution grids through coordinated re-phasing of grid-connected rooftop PV systems. The optimum phase combination of grid-connected rooftop PV systems is determined from the modified discrete bacterial foraging optimization algorithm (DBFOA) at fixed time intervals. The DBFOA takes smart meter measurements such as load demands and PV generations as the inputs to determine the optimum phase configuration such that the resulting phase combination minimizes the overall voltage unbalance in the network, subject to various operating and network parameters. In order to perform automatic PV re-phasing, a PV re-phasing switch is introduced. This can connect to the output of the single-phase PV inverters to enable the PV re-phasing. To nullify the transient time associated with the automatic re-phasing switch, a half-bridge inverter arrangement is also proposed.

In order to demonstrate the effectiveness of the proposed re-phasing strategy, the PV re-phasing algorithm was simulated on a real LV distribution network. The time-varying nature of loads and solar PV was considered using the hourly load and PV generation profiles. The results show that the proposed re-phasing strategy can significantly reduce the voltage unbalance well below the 1% threshold line as compared to the fixed phase configuration during the daytime where PV penetration is high. Thereby the proposed PV re-phasing strategy facilitates utility providers to allow more rooftop solar systems into LV networks. The proposed case studies demonstrate that PV re-phasing technique can increase the renewable energy penetration into the considered LV network by 77%.

The main advantage of the proposed PV re-phasing technique compared to existing load and feeder reconfiguration techniques is that this method only deals with single-phase PV systems. Hence, it will not create any impact on supply reliability. Furthermore, the initial cost for installation of PV re-phasing switches, and other indirect costs such as customer interruption cost and reliability cost are significantly minimal, as compared to existing state-of-the-art DFR and phase balancing techniques. The initial cost for installing PV re-phasing switches can be recovered by the long-term economic benefits due to the improvement in usable PV capacity and due to the possibility of operating the system in a near balanced condition. Further, compared to the rephasing arrangements reported in the literature, i.e. introducing rephasing switches to all loads, the cost incurred due to the introduction of re-phasing switches, only to PV plants, makes the proposed method more cost-effective.

The main limitation of this work is that the proposed PV re-phasing method is only effective during the daytime and cannot make a significant reduction to the unbalance factor at night. However, the Volt-Var (Q-control) control can be used to reduce voltage unbalance and improve power quality during night-time, because PV inverters can supply reactive power (Q) to the grid up to their rated capacity at night. Therefore, combining the PV re-phasing technique with Volt-Var control would be an ideal solution and is considered as future research work. In addition, it should be noted that the unbalance reduction capability of the proposed PV re-phasing technique greatly depends on the number of grid-connected rooftop solar systems in the distribution network. Therefore, for

distribution systems with a smaller number of grid-connected rooftop solar systems, the number of possible configurations is limited, thus, optimization via fine-tuning through re-phasing is not possible as the number of configurations to adjust is limited. Further, a communication protocol needs to be developed to ensure that the PV re-phasing command issued by the algorithm is actually performed by the switches, because if one/several re-phasing switch commands are not executed due to communication errors or other technical issues, the system can be at a worse state than before. Therefore, improvements should be made to address these, before implementing the proposed PV re-phasing technique in an actual network.

Even though the proposed re-phasing algorithm concentrates on mitigation of voltage unbalance, it is also possible to modify the objective function to minimize the number of PV re-phasings required for each PV re-phasing operation as well. Furthermore, additional research is required to determine the optimal timing for PV re-phasing operations and the effectiveness of a hybrid algorithm based on PV and load re-phasing techniques.

8. Acknowledgment

We would like to acknowledge the financial support provided by the National Science Foundation (NSF), Sri Lanka (research grant no: RG/2018/EA & ICT/01).

9. References

- [1] Jadeja K. Major Technical issues with increased PV penetration on the existing electrical grid. Murdoch University, 2012. <https://doi.org/https://core.ac.uk/download/pdf/11241964.pdf>.
- [2] Lu H, Zhao W. Effects of particle sizes and tilt angles on dust deposition characteristics of a ground-mounted solar photovoltaic system. *Appl Energy* 2018;220:514–26. <https://doi.org/10.1016/j.apenergy.2018.03.095>.
- [3] Peters L, Madlener R. Economic evaluation of maintenance strategies for ground-mounted solar photovoltaic plants. *Appl Energy* 2017;199:264–80. <https://doi.org/10.1016/j.apenergy.2017.04.060>.
- [4] Zhou Y, Chang F-J, Chang L-C, Lee W-D, Huang A, Xu C-Y, et al. An advanced complementary scheme of floating photovoltaic and hydropower generation flourishing water-food-energy nexus synergies. *Appl Energy* 2020;275:115389. <https://doi.org/10.1016/j.apenergy.2020.115389>.
- [5] Wang Q, Zhu Z, Wu G, Zhang X, Zheng H. Energy analysis and experimental verification of a solar freshwater self-produced ecological film floating on the sea. *Appl Energy* 2018;224:510–26. <https://doi.org/10.1016/j.apenergy.2018.05.010>.
- [6] Hong T, Lee M, Koo C, Jeong K, Kim J. Development of a method for estimating the rooftop solar photovoltaic (PV) potential by analyzing the available rooftop area using Hillshade analysis. *Appl Energy* 2017;194:320–32. <https://doi.org/10.1016/j.apenergy.2016.07.001>.
- [7] Cole W, Lewis H, Sigrin B, Margolis R. Interactions of rooftop PV deployment with the

- capacity expansion of the bulk power system. *Appl Energy* 2016;168:473–81. <https://doi.org/10.1016/j.apenergy.2016.02.004>.
- [8] Carpinelli G, Mottola F, Proto D, Varilone P. Minimizing unbalances in low-voltage microgrids: Optimal scheduling of distributed resources. *Appl Energy* 2017;191:170–82. <https://doi.org/10.1016/j.apenergy.2017.01.057>.
- [9] Zehir MA, Batman A, Sonmez MA, Font A, Tsiamitros D, Stimoniariis D, et al. Impacts of microgrids with renewables on secondary distribution networks. *Appl Energy* 2017;201:308–19. <https://doi.org/10.1016/j.apenergy.2016.12.138>.
- [10] Wang L, Yan R, Saha TK. Voltage regulation challenges with unbalanced PV integration in low voltage distribution systems and the corresponding solution. *Appl Energy* 2019;256:113927. <https://doi.org/10.1016/j.apenergy.2019.113927>.
- [11] Ma K, Li R, Hernando-Gil I, Li F. Quantification of Additional Reinforcement Cost from Severe Three-Phase Imbalance. *IEEE Trans Power Syst* 2017;32:4143–4. <https://doi.org/10.1109/TPWRS.2016.2635383>.
- [12] Yaghoobi J, Islam M, Mithulananthan N. Analytical approach to assess the loadability of unbalanced distribution grid with rooftop PV units. *Appl Energy* 2018;211:358–67. <https://doi.org/10.1016/j.apenergy.2017.11.030>.
- [13] Islam MR, Lu H, Hossain MJ, Li L. Mitigating unbalance using distributed network reconfiguration techniques in distributed power generation grids with services for electric vehicles: A review. *J Clean Prod* 2019;239:117932. <https://doi.org/10.1016/j.jclepro.2019.117932>.
- [14] Ramos-figueroa O, Quiroz-castellanos M, Mezura-montes E. Metaheuristics to solve grouping problems: A review and a case study. *Swarm Evol Comput* 2020;53:100643. <https://doi.org/10.1016/j.swevo.2019.100643>.
- [15] Fukami T, Onchi T, Naoe N, Hanaoka R. Compensation for neutral current harmonics in a three-phase four-wire system by a synchronous machine. *IEMDC 2001. IEEE Int. Electr. Mach. Drives Conf. (Cat. No.01EX485)*, IEEE; n.d., p. 466–70. <https://doi.org/10.1109/IEMDC.2001.939346>.
- [16] Jou H-L, Wu J-C, Wu K-D, Chiang W-J, Chen Y-H. Analysis of Zig-Zag Transformer Applying in the Three-Phase Four-Wire Distribution Power System. *IEEE Trans Power Deliv* 2005;20:1168–73. <https://doi.org/10.1109/TPWRD.2005.844281>.
- [17] Enjeti P, Shireen W, Packebush P, Pitel I. Analysis and design of a new active power filter to cancel neutral current harmonics in three phase four wire electric distribution systems. *Conf. Rec. 1993 IEEE Ind. Appl. Conf. Twenty-Eighth IAS Annu. Meet., IEEE*; n.d., p. 939–46. <https://doi.org/10.1109/IAS.1993.299011>.
- [18] Singh B, Jayaprakash P, Kothari DP. A T-Connected Transformer and Three-leg VSC Based DSTATCOM for Power Quality Improvement. *IEEE Trans Power Electron* 2008;23:2710–8. <https://doi.org/10.1109/TPEL.2008.2004273>.
- [19] Jayaprakash P, Singh B, Kothari DP. Three-Phase 4-Wire DSTATCOM Based on H-Bridge VSC with a Star/Hexagon Transformer for Power Quality Improvement. 2008 IEEE Reg.

- 10 Third Int. Conf. Ind. Inf. Syst., IEEE; 2008, p. 1–6. <https://doi.org/10.1109/ICIINFS.2008.4798378>.
- [20] Quinn CA, Mohan N. Active filtering of harmonic currents in three-phase, four-wire systems with three-phase and single-phase nonlinear loads. [Proceedings] APEC '92 Seventh Annu. Appl. Power Electron. Conf. Expo., IEEE; n.d., p. 829–36. <https://doi.org/10.1109/APEC.1992.228328>.
- [21] Jou H-L, Wu K-D, Wu J-C, Li C-H, Huang M-S. Novel power converter topology for three-phase four-wire hybrid power filter. IET Power Electron 2008;1:164. <https://doi.org/10.1049/iet-pel:20070171>.
- [22] Sreenivasarao D, Agarwal P, Das B. Neutral current compensation in three-phase, four-wire systems: A review. Electr Power Syst Res 2012;86:170–80. <https://doi.org/10.1016/j.epsr.2011.12.014>.
- [23] Omar AI, Abdel Aleem SHE, El-Zahab EEA, Algablawy M, Ali ZM. An improved approach for robust control of dynamic voltage restorer and power quality enhancement using grasshopper optimization algorithm. ISA Trans 2019;95:110–29. <https://doi.org/10.1016/j.isatra.2019.05.001>.
- [24] Kashem MA, Ganapathy V, Jasmon GB. Network reconfiguration for load balancing in distribution networks. IEE Proc - Gener Transm Distrib 1999;146:563. <https://doi.org/10.1049/ip-gtd:19990694>.
- [25] Babu PR, Kumar KA, Teja GC. New heuristic search approach to enhance the distribution system load balance. 2013 Int. Conf. Power, Energy Control, IEEE; 2013, p. 159–64. <https://doi.org/10.1109/ICPEC.2013.6527642>.
- [26] Babu PR, Shenoy R, Ramya N, Soujanya, Shetty S. Implementation of ACO technique for load balancing through reconfiguration in electrical distribution system. 2014 Annu. Int. Conf. Emerg. Res. Areas Magn. Mach. Drives, IEEE; 2014, p. 1–5. <https://doi.org/10.1109/AICERA.2014.6908233>.
- [27] Yuehao Y, Zhongqing Z, Wei B, Jun X, Limin Q, Yaoheng D. Optimal distribution network reconfiguration for load balancing. 2016 China Int. Conf. Electr. Distrib., vol. 2016- Septe, IEEE; 2016, p. 1–4. <https://doi.org/10.1109/CICED.2016.7576313>.
- [28] Taher SA, Karimi MH. Optimal reconfiguration and DG allocation in balanced and unbalanced distribution systems. Ain Shams Eng J 2014;5:735–49. <https://doi.org/10.1016/j.asej.2014.03.009>.
- [29] Fu-Yuan Hsu, Men-Shen Tsai. A Multi-Objective Evolution Programming Method for Feeder Reconfiguration of Power Distribution System. Proc. 13th Int. Conf. on, Intell. Syst. Appl. to Power Syst., vol. 2005, IEEE; 2005, p. 55–60. <https://doi.org/10.1109/ISAP.2005.1599241>.
- [30] Vitor TS, Vieira JCM. Optimal voltage regulation in distribution systems with unbalanced loads and distributed generation. 2016 IEEE Innov. Smart Grid Technol. - Asia, IEEE; 2016, p. 942–7. <https://doi.org/10.1109/ISGT-Asia.2016.7796512>.
- [31] Nara K, Mishima Y, Satoh T. Network reconfiguration for loss minimization and load

- balancing. 2003 IEEE Power Eng. Soc. Gen. Meet. (IEEE Cat. No.03CH37491), vol. 4, IEEE; 2003, p. 2413–8. <https://doi.org/10.1109/PES.2003.1271019>.
- [32] Qin Zhou, Shirmohammadi D, Liu W-HE. Distribution feeder reconfiguration for service restoration and load balancing. *IEEE Trans Power Syst* 1997;12:724–9. <https://doi.org/10.1109/59.589664>.
- [33] Tolabi HB, Ali MH, Shahrin Bin Md Ayob, Rizwan M. Novel hybrid fuzzy-Bees algorithm for optimal feeder multi-objective reconfiguration by considering multiple-distributed generation. *Energy* 2014;71:507–15. <https://doi.org/10.1016/j.energy.2014.04.099>.
- [34] Ke Y-L, Chen C-S, Kang M-S, Wu J-S, Lee T-E. Power Distribution System Switching Operation Scheduling for Load Balancing by Using Colored Petri Nets. *IEEE Trans Power Syst* 2004;19:629–35. <https://doi.org/10.1109/TPWRS.2003.821433>.
- [35] Lin C-H. Distribution network reconfiguration for load balancing with a coloured Petri net algorithm. *IEE Proc - Gener Transm Distrib* 2003;150:317. <https://doi.org/10.1049/ip-gtd:20030199>.
- [36] Ji H, Wang C, Li P, Zhao J, Song G, Ding F, et al. An enhanced SOCP-based method for feeder load balancing using the multi-terminal soft open point in active distribution networks. *Appl Energy* 2017;208:986–95. <https://doi.org/10.1016/j.apenergy.2017.09.051>.
- [37] Diaaeldin I, Abdel Aleem S, El-Rafei A, Abdelaziz A, Zobaa AF. Optimal Network Reconfiguration in Active Distribution Networks with Soft Open Points and Distributed Generation. *Energies* 2019;12:4172. <https://doi.org/10.3390/en12214172>.
- [38] Zhai HF, Yang M, Chen B, Kang N. Dynamic reconfiguration of three-phase unbalanced distribution networks. *Int J Electr Power Energy Syst* 2018;99:1–10. <https://doi.org/10.1016/j.ijepes.2017.12.027>.
- [39] Santos SF, Fitiwi DZ, Cruz MRM, Cabrita CMP, Catalão JPS. Impacts of optimal energy storage deployment and network reconfiguration on renewable integration level in distribution systems. *Appl Energy* 2017;185:44–55. <https://doi.org/10.1016/j.apenergy.2016.10.053>.
- [40] Kaveh MR, Hooshmand R-A, Madani SM. Simultaneous optimization of re-phasing, reconfiguration and DG placement in distribution networks using BF-SD algorithm. *Appl Soft Comput* 2018;62:1044–55. <https://doi.org/10.1016/j.asoc.2017.09.041>.
- [41] Soltani SH, Rashidinejad M, Abdollahi A. Dynamic phase balancing in the smart distribution networks. *Int J Electr Power Energy Syst* 2017;93:374–83. <https://doi.org/10.1016/j.ijepes.2017.06.016>.
- [42] Jinxiang Zhu, Mo-Yuen Chow, Fan Zhang. Phase balancing using mixed-integer programming [distribution feeders]. *IEEE Trans Power Syst* 1998;13:1487–92. <https://doi.org/10.1109/59.736295>.
- [43] Zhu J, Bilbro G, Mo-Yuen Chow. Phase balancing using simulated annealing. *IEEE Trans Power Syst* 1999;14:1508–13. <https://doi.org/10.1109/59.801943>.
- [44] Kuo C-C, Chao Y-T. Energy management based on AM/FM/GIS for phase balancing

- application on distribution systems. *Energy Convers Manag* 2010;51:485–92. <https://doi.org/10.1016/j.enconman.2009.10.011>.
- [45] Chitra R, Neelaveni R. A realistic approach for reduction of energy losses in low voltage distribution network. *Int J Electr Power Energy Syst* 2011;33:377–84. <https://doi.org/10.1016/j.ijepes.2010.08.033>.
- [46] Hooshmand RA, Soltani S. Fuzzy Optimal Phase Balancing of Radial and Meshed Distribution Networks Using BF-PSO Algorithm. *IEEE Trans Power Syst* 2012;27:47–57. <https://doi.org/10.1109/TPWRS.2011.2167991>.
- [47] Gray MK, Morsi WG. Economic assessment of phase reconfiguration to mitigate the unbalance due to plug-in electric vehicles charging. *Electr Power Syst Res* 2016;140:329–36. <https://doi.org/10.1016/j.epr.2016.06.008>.
- [48] Das CK, Bass O, Kothapalli G, Mahmoud TS, Habibi D. Optimal placement of distributed energy storage systems in distribution networks using artificial bee colony algorithm. *Appl Energy* 2018;232:212–28. <https://doi.org/10.1016/j.apenergy.2018.07.100>.
- [49] BARRY WW. *Power Electronics: devices, drives, applications and passive components* 1992.
- [50] Dinesh C, Welikala S, Liyanage Y, Ekanayake MPB, Godaliyadda RI, Ekanayake J. Non-intrusive load monitoring under residential solar power influx. *Appl Energy* 2017;205:1068–80. <https://doi.org/10.1016/j.apenergy.2017.08.094>.
- [51] Welikala S, Thelasingha N, Akram M, Ekanayake PB, Godaliyadda RI, Ekanayake JB. Implementation of a robust real-time non-intrusive load monitoring solution. *Appl Energy* 2019;238:1519–29. <https://doi.org/10.1016/j.apenergy.2019.01.167>.
- [52] Andreadou N, Kotsakis E, Masera M. Smart Meter Traffic in a Real LV Distribution Network. *Energies* 2018;11:1156. <https://doi.org/10.3390/en11051156>.
- [53] Chaminda Bandara WG, Almeida D, Godaliyadda RI, Ekanayake MP, Ekanayake J. A complete state estimation algorithm for a three-phase four-wire low voltage distribution system with high penetration of solar PV. *Int J Electr Power Energy Syst* 2021;124:106332. <https://doi.org/10.1016/j.ijepes.2020.106332>.
- [54] Wen H, Cheng D, Teng Z, Guo S, Li F. Approximate Algorithm for Fast Calculating Voltage Unbalance Factor of Three-Phase Power System. *IEEE Trans Ind Informatics* 2014;10:1799–805. <https://doi.org/10.1109/TII.2014.2327485>.
- [55] K.M. Passino. Biomimicry of bacterial foraging for distributed optimization and control. *IEEE Control Syst* 2002;22:52–67. <https://doi.org/10.1109/MCS.2002.1004010>.
- [56] Das S, Biswas A, Dasgupta S, Abraham A. *Bacterial Foraging Optimization Algorithm: Theoretical Foundations, Analysis, and Applications*. Found. Comput. Intell. Vol. 3. Stud. Comput. Intell., Berlin, Heidelberg: Springer-Verlag; 2009, p. 23–55. https://doi.org/10.1007/978-3-642-01085-9_2.
- [57] Kaveh MR, Hooshmand RA, Madani SM. Simultaneous optimization of re-phasing, reconfiguration and DG placement in distribution networks using BF-SD algorithm. *Appl*

- Soft Comput J 2018;62:1044–55. <https://doi.org/10.1016/j.asoc.2017.09.041>.
- [58] Devi S, Geethanjali M. Application of Modified Bacterial Foraging Optimization algorithm for optimal placement and sizing of Distributed Generation. *Expert Syst Appl* 2014;41:2772–81. <https://doi.org/10.1016/j.eswa.2013.10.010>.
- [59] Devabalaji KR, Ravi K, Kothari DP. Optimal location and sizing of capacitor placement in radial distribution system using Bacterial Foraging Optimization Algorithm. *Int J Electr Power Energy Syst* 2015;71:383–90. <https://doi.org/10.1016/j.ijepes.2015.03.008>.
- [60] Sathish Kumar K, Jayabarathi T. Power system reconfiguration and loss minimization for an distribution systems using bacterial foraging optimization algorithm. *Int J Electr Power Energy Syst* 2012;36:13–7. <https://doi.org/10.1016/j.ijepes.2011.10.016>.
- [61] Hooshmand R-A, Parastegari M, Morshed MJ. Emission, reserve and economic load dispatch problem with non-smooth and non-convex cost functions using the hybrid bacterial foraging-Nelder–Mead algorithm. *Appl Energy* 2012;89:443–53. <https://doi.org/10.1016/j.apenergy.2011.08.010>.